Cipolletti *et al. Cell Communication and Signaling* (2026) 24:83
https://doi.org/10.1186/s12964-025-02639-5

Cell Communication and Signaling

RESEARCH Open Access

The natural L370F ERα variant confers endocrine resistance and sensitivity to ATRA in metastatic breast cancer cells

Manuela Cipolletti[1], Claudia Bellucci[1], Marco Fiocchetti[1], Matic Pavlin[2], Alessandra Magistrato[3] and Filippo Acconcia[1*]

Abstract

Background Metastatic breast cancer (MBC) remains a major clinical challenge, particularly in estrogen receptor α (ERα)-positive patients who develop resistance to endocrine therapy (ET). While hotspot mutations such as Y537S in the ligand-binding domain (LBD) are well-characterized drivers of resistance, other ERα variants remain poorly studied. Understanding the molecular mechanisms underlying resistance in these variants is crucial for identifying novel therapeutic strategies. Here, we investigated the functional role of the L370F and E471D ERα variants, which are spatially close in the ERα structure.

Methods Stable overexpressing HEK293 cells and CRISPR/CAS9 engineered MCF-7 cells were generated and treated with 17β-estradiol (E2), fulvestrant (Ful) and all-trans retinoic acid (ATRA) to measure ERα stability, transcriptional activity and gene expression analyses using different cellular assays and RNASeq techniques. Direct in vitro measurement of ligand binding affinity to ERα were performed using the purified full-length wild type (wt) as well as L370F and Y537S ERα. In silico structural simulations were also performed to predict the structure of the mutated L370F ERα. Senescence analyses of MCF-7 and Y537S MCF-7 cells were performed using direct measurement β-galactosidase activity in vitro and in cell lines.

Results The L370F variant conferred resistance to Ful in terms of in vitro ERα binding, ERα transcriptional activity, receptor degradation and cell proliferation by modifying the folding of the receptor structure. Furthermore, L370F-expressing cells exhibited a hyperactive response to low doses of E2 and basally upregulated late estrogen responsive genes. Additionally, we found that both L370F and Y537S ERα variants displayed increased RARα expression, rendering them highly sensitive to ATRA. Notably, ATRA killed L370F-expressing cells and induced senescence in Y537S-expressing cells, highlighting mutation-specific responses.

Conclusions Our findings expand the understanding of ERα mutations beyond known hotspots, identifying L370F as a novel mutation contributing to ET resistance and further indicate the necessity to characterize all the less-studied ERα variants found in MBC. Furthermore, we demonstrate that ATRA selectively targets MBC cells harboring L370F and Y537S mutations, suggesting its potential as a mutation-specific therapeutic agent. These results support further investigation of ATRA in clinical settings to improve treatment strategies for ERα-mutant MBC.

*Correspondence:
Filippo Acconcia
filippo.acconcia@uniroma3.it

Full list of author information is available at the end of the article

Keywords Breast cancer, Estrogen receptor α, Endocrine resistance, ERα mutations, Fulvestrant, All-trans retinoic acid, Targeted therapy

Background

Breast cancer (BC) is the deadliest tumor type for women. Approximately 70% of BC cases express the estrogen receptor α (ERα), and patients with this form of the disease are effectively treated with endocrine therapy (ET) drugs (e.g., aromatase inhibitors - AIs, selective ER modulators – SERMs, and selective ER down-modulators – SERDs). However, 20–40% of these patients experience relapse and develop metastatic BC (MBC), which is resistant to the classic ET drugs (e.g., AIs; 4OH-tamoxifen – Tam) and is largely incurable [1]. BC cells can acquire resistance to ET drugs through multiple molecular mechanisms. Interestingly, in approximately 50% of ERα-expressing MBCs, ERα point mutations emerge and lead to a hyperactive ERα (e.g., Y537S), conferring specific proliferative advantages and mediating resistance to ET drugs [1].

The actual clinical strategies for MBC currently involve treating patients either with the second-line therapy drug fulvestrant (Ful), a SERD inducing ERα degradation, or with targeted agents (e.g., the CDK4/6 inhibitors palbociclib, ribociclib, or abemaciclib), which can be administered in combination with ET drugs [1].

Recently, novel antiestrogen drugs that bind either non-covalently or covalently to the Y537S ERα mutation, induce its degradation and block its hyperactive phenotype (e.g., the SERDs such as AZD9833, camizestrant; RAD-1901, elacestrant; GDC-9545, giredestrant; GDC-0927; the selective ERα covalent antagonists – SERCAs, H3B-5942; proteolysis targeting chimerics – PROTACs, such as ARV-471; complete estrogen receptor antagonists – CERANs, such as OP-1250), are currently undergoing clinical trials or have been recently approved (i.e., RAD-1901, elacestrant; LY3484356, imlunestrant;) [1–10].

In addition, we have demonstrated that 'antiestrogen-like' activities can be found in Food and Drug Administration (FDA) approved drugs that do not directly bind to ERα but determine its degradation. In particular, we have reported that cardiac glycosides, antivirals, and Chk1 inhibitors induce the degradation of the Y537S ERα variant, block its hyperactive phenotype, and prevent the proliferation of MBC cells expressing it when administered alone or in combination with either ET drugs or with CDK4/6 inhibitors [11–14]. Thus, a broad range of drugs could be used for the clinical treatment of MBC expressing the Y537S ERα [1].

To date, ~ 50 ERα point mutations have been identified in MBC patients and annotated in the free on line Cosmic and cBioPortal databases [15], all of which reduce their survival rates [15]. The most frequent and best-characterized variants map in one hotspot region within the receptor ligand-binding domain (LBD) (e.g., Y537S) [15]. However, many ERα variants fall outside this hotspot region and have been so far neglected. Recently, the initial characterization of some of them (V422del, G442R, F461V, S463P, L469V [16], and F404L/I/V [17]) revealed another hotspot within the LBD [16] and indicated that distinct mechanisms underlying uncontrolled proliferation [16] or resistance to ET drugs [17] can be operative in MBC.

In this study, we investigated the L370F and E471D ERα variants because we observed that, among the receptor point mutations found in MBC located within the LBD and annotated in the COSMIC and cBioPortal databases [15], the side chains of residues L370, laying on helix 4 (H4) and E471, laying within helix H10 [18] are facing each other in the LDB structure (Fig. 1A, yellow residues). Due to this spatial configuration, we hypothesized that they could represent a novel 3D-hotspot and, in turn, their single mutations in MBC could provide specific selective advantages to tumor cells (the double L370F/E471D mutation has not been identified in MBC patients).

Consistently, specific ERα cellular assays demonstrated that the L370F ERα variant is resistant to high doses of Ful and leads to a hyperactive response to low doses of 17β-estradiol (E2). Additionally, both the L370F and Y537S ERα variants exhibit high expression levels of retinoic acid receptor α (RARα) and all-trans retinoic acid (ATRA) induces cell death in the presence of the L370F ERα mutant and senescence in the presence of the Y537S ERα mutant.

These data establish that the L370F ERα variants confer distinct properties to MBC cells, highlighting ATRA as a potential ERα-variant-specific therapeutic agent for MBC driven by ERα function.

Materials and methods

Cell culture and reagents

HEK293 and MCF-7 cell lines were obtained from ATCC (USA), and all other cell lines used in this study were derived from these parental lines. Cells were maintained following the manufacturer's recommendations. The following reagents and antibodies were employed: 17β-estradiol (E2), DMEM (with or without phenol red), fetal calf serum, and charcoal-stripped fetal calf serum were purchased from Sigma-Aldrich (St. Louis, MO, USA). The Bradford protein quantification kit and HRP-conjugated secondary antibodies (anti-mouse and anti-rabbit) were obtained from Bio-Rad (Hercules, CA, USA).

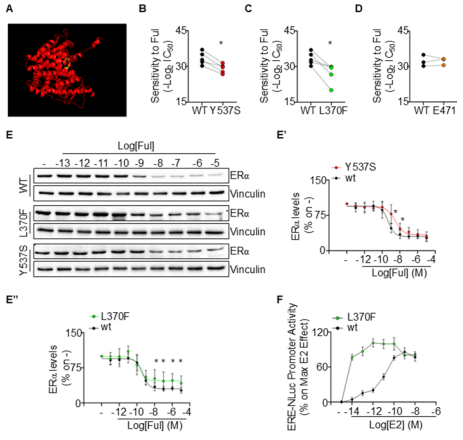

Fig. 1 Characterization of the fulvestrant effect in stable L370F and E471D ERα variants expressing HEK293 cells. **A** Structure of the wild type (wt) ERα ligand binding domain (pdb code: 1A52 [19]) where the L370 and E471 residues are highlighted in yellow. **B**-**D** Dose-response of ERα transcriptional activity have been performed in HEK293 cells stably expressing both the estrogen responsive element nanoluciferase (ERE-NLuc) reporter construct and the expression vectors encoding for the indicated ERα variants. Each dot represents the -Log_2 transformation of the inhibitory concentration 50 (IC_{50}) of the Ful effect in each cell line. Dotted lines indicate the two Ful IC_{50} obtained in the same experiment in which each condition was tested in triplicate. * indicates the significant differences calculated using the Student's t-test ($p < 0.05$). **E** Western blot and (**E'** and **E''**) relative densitometric analyses of ERα levels in HEK293 cells stably expressing both the ERE-NLuc reporter construct and the expression vectors encoding for the indicated ERα variants treated for 24 h with the indicated doses of fulvestrant (Ful). Each experiment was performed at least in triplicate and significant differences in the effect of Ful between the wt and mutant ERα expressing HEK293 cells were calculated using the Student's t-test (* indicates $p < 0.05$). **F** Dose-response of ERα transcriptional activity in HEK293 cells stably expressing both the ERE-NLuc reporter construct and the expression vectors encoding for the wt and L370F ERα treated with the indicated doses of 17β-estradiol (E2). Experiments were performed three times, and each condition was tested in triplicate

Primary antibodies against ERα (F-10, mouse), RARα (C-1, mouse), ASCL1 (D-7, mouse), CALCR (CT-R, 2F7, mouse), FABP5 (E-FABP, C-20, rabbit), and Caveolin-1 (N-20, rabbit) were obtained from Santa Cruz Biotechnology (Santa Cruz, CA, USA). Additional antibodies included anti-phospho ERα (Ser118, mouse), anti-phospho H2AX (rabbit), anti-PARP (rabbit), and anti-FASN (rabbit) from Cell Signaling Technology (USA). Anti-flag M2 (mouse), anti-vinculin (mouse) and anti-tubulin (mouse) antibodies were obtained from Sigma-Aldrich. Western blot chemiluminescence detection reagents were purchased from Bio-Rad. The following compounds were used in selected experiments: all-trans retinoic acid (ATRA), digoxin (Digo) and bafilomycin A1 from Sigma-Aldrich; fulvestrant (Ful), 4OH-tamoxifen (Tam), disulfiram, necrostatin, and ferrostatin from Selleck Chemicals (USA). The ERα Green Competitor Assay Kit (PolarScreen™, A15882) was obtained from Thermo Scientific. All other reagents were from Sigma-Aldrich and used without further purification, unless otherwise specified. Cell line authentication was confirmed by STR profiling performed by BMR Genomics (Italy).

ERα mutant CRISPR/CAS9 MCF-7 cell models

In this work we generated MCF-7 L370F cells using CRISPR/Cas9 technology employing an outsourced service (Cogentech in 2021). A clone (clone 3–78) was obtained with two correctly modified alleles (HDR alleles carrying the G/C mutation, which converts the TTG (L) codon into TTC (F), along with three synonymous mutations) and one allele with a single-nucleotide insertion, resulting in a frameshift and a premature stop codon immediately after the insertion. Details of the procedure are available upon request. CRISPR/Cas9 MCF-7 L370F cells were derived from parental MCF-7 commercially available purchased by ATCC (USA). We refer to these control cells as parental MCF-7 cells throughout the text. CRISPR/Cas9 Y537S MCF-7 cells were received from [20].

Cell manipulation for Western blot analyses

Cell manipulation, Western blotting Image acquisition and consequent manipulations including band quantitation have been described in detail in [21]. For studies of ERα and RARα interaction, stable HEK293 cell lines expressing HA- and His-tagged wild-type, L370F, and Y537S ERα were transiently transfected with the pcDNA plasmid encoding flag-tagged RARα (Addgene, USA) [22] using Lipofectamine 3000™ according to the manufacturer's instructions. Forty-eight hours after transfection, cells were lysed as described in [21], and 500 µg of proteins were incubated with Ni-beads (Thermo Scientific) for 1 h at 4 °C. After extensive washing with lysis buffer, proteins were eluted by boiling the resin for 5 min and then loaded onto a 7.5% SDS-PAGE gel. Western blotting was performed as described in [21].

Small interference RNA

For the small interference RNA (siRNA) experiments, cells were transfected with esiRNA [obtained from Sigma-Aldrich (St. Louis, MO, USA)] targeting the specific proteins of interest. The transfection procedure was conducted using Lipofectamine RNAi Max (Thermo Fisher), following established protocols described in [23].

Cell proliferation assays

The xCELLigence DP system (ACEA Biosciences, Inc., San Diego, CA) Multi-E-Plate station was utilized to measure the time-dependent response to the specified drugs by real-time cell analysis (RTCA), following previously reported protocols [21]. Synergy studies were conducted using Crystal Violet staining, as described in [21] at the time point where the control cells (i.e., untreated)

reached the confluency. The synergy was subsequently calculated using Combenefit freeware software [14].

Measurement of the cellular area

Following the indicated stimulation, phase-contrast images of MCF-7, L370F, and Y537S cells were randomly acquired using a ZEISS Axio Vert.A1 FL-LED fluorescence microscope (20× objective, 1× zoom) (Zeiss, Oberkochen, Germany). For cell area analysis, images were loaded into the FIJI distribution of the ImageJ program in their native format. Prior to analysis, brightness and contrast were adjusted using the "Brightness/Contrast" tool in FIJI to ensure optimal definition of the cell profile. Cellular contours were manually traced using the "Freehand Selection" tool to define the Region of Interest (ROI). Multiple ROIs were then selected from the ROI Manager, and the "Measure" tool under the "Analyze" menu was applied with the measurement parameter set to "Area", representing the surface area of the selected ROIs. The obtained values were reported as indicative of cell area in μm^2.

Measurement of Annexin V/Necrosis and caspase activity

For the measurement of Annexin V and necrosis, RealTime-Glo™ Annexin V Apoptosis and Necrosis assay (Promega, Madison, MA, USA) was used according to manufacturer's instruction. Briefly, 4,000 cells were plated in 96 well plates and treated with ATRA over the experimental period (72 h). Annexin V exposure and Necrosis activation were detected using a Tecan Spark Elisa reader by measuring luminescence and fluorescence, respectively. For the measurement of caspase 3/7, caspase 8 and caspase 9 activity, Caspase-Glo® Assay Systems (Promega, Madison, MA, USA) were used according to manufacturer's instruction. Briefly, 10,000 cells were plated in 96 well plates and treated with ATRA over the experimental period and luminescence was detected using a Tecan Spark Elisa reader.

Generation of stable cell lines and measurement of ERα and RARα transcriptional activity

The generation of HEK293 cells stably transfected with a reporter gene containing an estrogen response element (ERE) controlling the expression of nanoluciferase (NLuc)-PEST was done using the selection methods and the reagents described in [24, 25]. These cell lines were then transfected with the pcDNA His HA wild type (wt), L370F and Y537S ERα and selected using neomycin. To generate the pcDNA His HA wt, and Y537S ERα, the pcDNA-HA-ERα [26] and the pcDNA-HA-Y537S ERα [26] were purchased from Addgene (USA) and digested with BamHI and ApaI to excide the receptor ORFs. The fragments were ligated into pcDNA His vector sites. To generate the pcDNA His HA L370F ERα, site-directed mutagenesis was performed on the pcDNA His HA ERα using the following forward 5'-gtgccaggctttgtggattttaccctccatgatcaggtccaccttc-3' and reverse 5'-cacggtccgaaacacctaaaatgggaggtactagtccaggtggaag-3' primers and using the QuickChange Lightning kit from Agilent (Santa Clara, CA, USA). All the resulting plasmids were sequence verified.

The generation of L370F MCF-7 cells stably transfected with a reporter gene containing the ERE sequence controlling the expression of NLuc-PEST was done using the selection methods and the reagents described in [24, 25]. This cell line together with the corresponding parental and Y537S MCF-7 ERE-NLuc cells were used to measure the ERα transcriptional activity as previously reported [24, 25].

To generate the parental, L370F and Y537S MCF-7 cells stably expressing a reporter gene containing an retinoic acid response element (RARE) controlling the expression of NLuc-PEST, the plasmid pGL2Basic_Neo_RARE-NLuc-PEST was transfected and the cell lines were selected as previously reported [24, 25]. To generate the plasmid pGL2Basic_Neo_RARE-NLuc-PEST, the RARE cassette was KpnI and HindIII excised from the pGL3-RARE-luciferase [27] purchased from Addgene (USA) and ligated into the corresponding restriction sites in the pGL2Basic_Neo_NLuc-PEST [24, 25].

Gene arrays and RNASeq analyses

Gene arrays analyses were conducted as described in [21]. RNASeq and the relative initial data analyses were performed by Novogene (Cambridge, UK) as an outsourced service. Briefly, three replicates of sub-confluent growing parental, L370F and Y537S MCF-7 cells were pelleted, and sent in dry ice for analysis to Novogene, which performed RNA extraction, quality control, mRNA library preparation (polyA enrichment) and sequencing using the NovaSeq X Plus Series (PE150) (6G raw data per sample) following by standard analysis (i.e., data quality control and data filtering, mapping to reference genome, gene expression quantitation and correlation analysis, differential expression analysis, enrichment analysis of differential expressed genes, GSEA enrichment analysis of expressed genes, protein-protein interaction analysis of differential expressed genes, oncogene functional annotation of differential expressed genes, alternative splicing quantification and differential analysis, SNP/InDel analysis and fusion gene analysis).

Full-length ERα purification from Expi293F cells

To generate the plasmid pcDNA 3.1_ ERα_TEV_TWIN STREP TAG, the TEV_TWIN STREP TAG was PCR amplified from the pcDNA3.1 GIL-11 myc TEV TwinStrep [28] purchased from Addgene (USA) using the following forward

5'-cggggtaccccgagcgcgtggagccatccgcagt-3' and reverse 5'-cgcggatccgcgtttttcaaactgcggatggct-3' primers. The fragment was EcoRI and XhoI digested and subcloned in pcDNA 3.1 to obtain the pcDNA 3.1_TEV_TWIN STREP TAG. Wild type , L370F and Y537S ERα were PCR amplified using pcDNA His HA wt, L370F and Y537S ERα plasmids as templates and the following forward 5'-cgcggatccgcgatgaccatgaccctccacaccaaagcatct-3' and reverse 5'-ccggaattccgggaccgtggcagggaaaccctc-3' primers. The resulting fragments were BamHI and EcoRI digested and subcloned into the corresponding restriction sites in the pcDNA 3.1_TEV_TWIN STREP TAG. The plasmids were then sequence-verified.

Transfection of the pcDNA 3.1_ ERα_TEV_TWIN STREP TAG encoding for the wt, L370 and Y537S receptor fused in frame with the TWIN STREP TAG (Molecular weight = 70,7 KDa, corresponding to 66,0 KDa of the ERα and 4,7 KDa of the TWIN STREP TAG) was conducted in Expi293F cells and performed by the National Facilities at the Human Technopole (Milan, Italy) as a service. Access to the Biomass Production Unit service @ the Human Technopole (Milan, Italy) was granted following a competitive selection procedure (Project ID 1771263). Expi293F cells were transfected at a density of 2–3 × 10^6 cells/ml using a modified PEI (polyethylenimine) protocol, with 1.1 mg of plasmid DNA and 3 mg of PEI per each liter of cell culture. A total of 10 L of Expi293F cells for each construct was transfected. After transfection cells have been grown in a Multitron shaker (Infors HT, Bottmingen, Switzerland) for additional 72 h. The cell suspension was divided into aliquots of 500 ml and then centrifuged at 1000 rcf, at 4 °C, for 10 min. The 500 ml cell pellets were then washed with PBS, the centrifugation was repeated and the supernatant discarded. The resulting pellets were stored at −80 °C until protein purification (see below).

A pellet of 500 ml of Expi293F cells was resuspended in 50 ml of the following lysis buffer 100 mM TrisHCl pH 8, 150 mM NaCl, 2% Triton X100, 10% Glycerol, 1mM EDTA, 10 mM $MgCl_2$, 1 mM ATP, 2 mM DTT, 10 µM Mg-132, 1mM PMSF and protease inhibitor cocktail and left on ice for 10 min. The volume was then centrifuged in 2 ml eppendorf tubes for 5 min at 4 °C at 10,000 rpm. The supernatant was loaded three times on a 3 ml gravity column Strep-Tactin®XT 4Flow® 50% suspension [IBA-Lifescience (Gottingen, Germany)] packed o.n. at 4 °C. After washing the column with > 50 ml of wash buffer (100 mM TrisHCl pH 8, 150 mM NaCl, 1 mM EDTA) 14 fractions of 1 ml were eluted with 100 mM TrisHCl pH 8, 150 mM NaCl, 1 mM EDTA, 50 mM biotin. The eluate was then concentrated in 50 KDa cut-off Amicon® Ultra [obtained from Sigma-Aldrich (St. Louis, MO, USA)] up to 500–800 µl. The purity of the purified ERα was evaluated by staining an SDS-PAGE gel with InstaBlue Protein Stain Solution (CliniScience, Italy). Receptor amount and purity was calculated in reference to a standard curve of bovine serum albumin (Supplementary Fig. 1 A). The final yield was in the µM range per each receptor.

In vitro ERα binding assay

The in vitro ERα binding assay employed a fluorescence polarization (FP) method to assess the binding affinity of 17β-estradiol (E2), and fulvestrant (Ful) with commercially available recombinant ERα and the purified full length wild type (wt), L370F and Y537S ERα-TWIN STREP TAG purified from Expi293F cells as described above. The FP assay was done as reported in [21]. Briefly, measurement has been performed using different doses of the test compounds in a final assay reaction that contained the above described ERα (50 nM - Supplementary Fig. 1B) and fluomone ES2 (4.5 nM) in ERα binding buffer (Thermo Scientific). Each sample was measured in quadruplicate in black 384 multiwell plates and the experiment was repeated twice. The assay was incubated for 2 h in the dark at room temperature before reading on a Tecan Spark Elisa reader. The calculation of the K_i was obtained from the apparent IC_{50} of the compound toward each receptor by performing the calculation as described in [29]. Briefly, we applied a modified Cheng-Prusoff equation [30] [Ki = (apparent IC_{50} * $K_{dFluomoneES2}$)/[Fluomone ES2] * ([Fluomone ES2] * $K_{dFluomoneES2}$)] to take into consideration the K_d of the fluomone ES2 toward the receptors (i.e., 18 nM) and the concentration of the flouomone ES2 used in the assay.

Classical molecular dynamics simulations

Three different ERα systems were prepared, namely the wild type , L370F, and E471D ERα with fulvestrant inside the binding cavity. The L370F and E471D model systems were prepared by mutating corresponding residues in the wt variant. ERα structures were prepared based on the wt ERα-fulvestrant complex from the study by Pavlin et al. 2018 [18].

500 ns-long simulations were performed for each system using Amber20 code [31]. FF19SB force field was used for the description of protein [32], which was placed in the cubic simulation box solvated with up to ~ 37,000 TIP3P water molecules, making sure that the distance between solute and edge of the box was at least 12 Å. For the description of fulvestrant same parameters as in ref [18]. were used. Each system was energy minimized by 20,000 steps using the steepest descent algorithm, followed by 30,000 steps of conjugate gradient. This was followed by the canonical NVT equilibration performed in 4 runs of 10,000 steps, with the constraints on the solute gradually releasing (from 100 kcal mol^{-1} $Å^{-2}$ in first run to 60 kcal mol^{-1} $Å^{-2}$ and 30 kcal mol^{-1} $Å^{-2}$ in the second and third run, respectively, while the fourth run was

performed without constraints) and the system was gradually heated to 293 K. Subsequently, NPT equilibration at 1 bar was carried out in two successive runs of 100,000 steps each. During the first run, the solute was restrained with a force constant of 20 kcal mol^{-1} $Å^{-2}$ and in the second run the constraint was released. Production runs were performed with periodic boundary conditions and electrostatic interaction were considered using Particle Mesh Ewald method [33] at 293 K and 1 bar by coupling to the Langevin thermostat [34] and Berendsen barostat [35]. In all simulations all bond lengths involving hydrogen atoms were constrained using SHAKE algorithm [36] to achieve a time step of 2 fs.

Analyses (namely RMSD, hydrogen bond (H-bond) analysis, clustering and cross correlation anaylsis) on the equilibrated part of trajectories, from 200 to 500 ns, were performed using AmberTools22 [37].

β-Galactosidase activity

β-Galactosidase activity was assessed using the Beta-Glo® assay system (Promega, Madison, MA, USA) following the manufacturer's guidelines. In brief, 2000 cells were seeded in 96-well plates and treated at the designated time point as specified. Luminescence was then read at Tecan Spark Elisa reader. Each condition was tested in triplicate. Replica plates were also used to normalize the experiment for cell number by using Crystal Violet staining, as described above. Detection of activity at pH 6, a known characteristic of senescent cells was performed the Senescence β-galactosidase staining kit (Cell Signaling, Technology Danvers, MA, USA) according to manufacturer's instructions. The experiment was performed twice triplicate.

Statistical analysis

Statistical analysis was conducted as detailed in been described in detail in [20].

Results

Evaluation of the sensitivity to Ful and E2 of HEK293 cells expressing L370F and E471D ERα variants

Since the ERα variants found in MBC are selected following administration of first-line ET drugs such as AI and/or Tam, MBC patients are typically treated with the second-line ET drug Ful [1].

To investigate whether the L370F and E471D ERα variants are resistant to this antiestrogen, we initially generated isogenic pooled stable HEK293 cell lines (ERα-negative cells) [38] co-expressing a reporter construct containing the estrogen response element (ERE) regulating a nanoluciferase gene (ERE-NLuc) [24, 25, 39]. Additionally, we introduced expression vectors encoding the L370F and E471D ERα variants fused with an *N*-terminal double tag (HA and His tag). As controls, we generated isogenic pooled stable HEK293 cell lines expressing wild type (wt) ERα and the hyperactive Y537S ERα mutant [20].

Dose-response analyses were conducted to evaluate the effectiveness of Ful in decreasing basal ERα transcriptional activity. Cells were treated with varying doses of Ful (10^{-13}M to 10^{-5}M) for 24 h, and the relative inhibitory concentration 50 (IC_{50}) was calculated. To evaluate the sensitivity of each cell line (wt, L370F, E471D, and Y537S ERα-expressing HEK293 cells) to Ful, the IC_{50} values were mathematically transformed to -Log_2 and plotted. As shown in Fig. 1B, HEK293 cells expressing the Y537S ERα mutant exhibited significantly reduced sensitivity to Ful, as expected [20]. Interestingly, while HEK293 cells expressing the E471D ERα mutant showed similar sensitivity to Ful as the wt ERα-expressing cells (Fig. 1D), the L370F ERα mutant cells displayed reduced sensitivity to Ful's inhibitory effect on receptor transcriptional activity compared to wt ERα cells (Fig. 1C). These data suggest that the L370F, but not the E471D ERα mutation, impairs Ful's ability to inhibit receptor transcriptional activity. Therefore, the E471D ERα mutant was excluded from further analysis.

Next, we evaluated Ful's capacity to induce ERα degradation in HEK293 cells expressing wt, L370F, and Y537S ERα mutants. Western blot (WB) analyses were conducted after 24-hour treatments with varying doses of Ful (10^{-13}M to 10^{-5}M) and Ful-induced receptor degradation in all cell lines was tested. As previously reported [20], the Y537S mutation reduced Ful-induced receptor degradation compared to wt ERα cells (Fig. 1E and E'). Interestingly, in HEK293 cells expressing the L370F mutant, higher doses of Ful (10^{-8}M to 10^{-5}M) were less effective in inducing receptor degradation as compared to wt ERα containing cells (Fig. 1E and E"). These results indicate that the L370F ERα mutation hinders Ful's ability to induce receptor degradation.

Similarly to the Y537S ERα mutant, many other point mutations located within the LBD lead to constitutively hyperactive ERα by causing structural changes that mimic the E2-activated conformation [40]. We then investigated the effect of E2 on the transcriptional activity of both wt and L370F ERα. HEK293 cells were treated with varying doses of E2 (10^{-14}M to 10^{-8}M) for 24 h, and transcriptional activity was measured. No significant differences in basal transcriptional activity were detected between wt and L370F receptors, and E2 induced a dose-dependent increase in transcriptional activity in both cell types (Fig. 1F). Nevertheless, at low doses of E2 (from 10^{-14}M to 10^{-10}M), the L370F ERα exhibited enhanced transcriptional activity as compared to its wt counterpart (Fig. 1F). These findings suggest that the L370F ERα mutation enhances the responsiveness of ERα to low doses of E2, increasing receptor transcriptional activity.

Evaluation of ful sensitivity in parental, L370F and Y573S CRISPR/CAS9-engineered MCF-7 cells

Previous results suggest that the L370F variant found in MBC may confer resistance to Ful treatment and promote hyperactivity in response to E2 in cells expressing this mutation. Consequently, cells expressing the L370F receptor mutation may evade the effects of ET drugs while continuing to proliferate under the influence of E2. To test this hypothesis, we generated a CRISPR/CAS9 knock-in L370F-mutated MCF-7 cell line that exclusively expresses the mutated receptor and studied them together with parental MCF-7 (i.e., commercially available MCF-7 cells) and Y537S MCF-7 cells (received from [20]) (please see also Material and Method section).

Initial experiments were conducted to validate the findings from stable HEK293 cells. The ability of Ful to induce ERα degradation was assessed through WB analysis in parental, L370F, and Y537S MCF-7 cells treated for 24 hours with varying doses of Ful (10^{-14}M to 10^{-6}M). As shown in Fig. 2A and A', Ful induced dose-dependent ERα degradation in all cell lines tested. As expected [20], the ability of Ful to degrade ERα was reduced in Y537S MCF-7 cells (Fig. 2A and A'). Notably, in L370F MCF-7 cells, high doses of Ful (10^{-7}M to 10^{-6}M) were less effective at inducing receptor degradation as compared to parental MCF-7 cells (Fig. 2A and A').

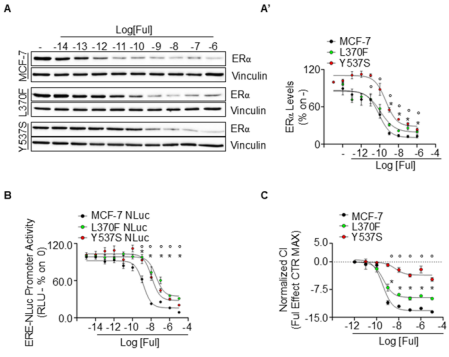

Fig. 2 Characterization of the fulvestrant effect in CRISPR/CAS9 engineered L370F MCF-7 cells. **A** Western blot and (**A'**) relative densitometric analyses of ERα levels in parental and CRISPR/CAS9 engineered L370F and Y537S MCF-7 cells treated for 24 h with the indicated doses of fulvestrant (Ful). Each experiment was performed at least in triplicate and significant differences in the effect of Ful between the parental and L370F ERα expressing MCF-7 cells (* indicates $p < 0.05$) and the Y537S MCF-7 cells (° indicates $p < 0.05$) were calculated using the Student's t-test. **B** Dose-response of ERα transcriptional activity in parental and CRISPR/CAS9 engineered L370F and Y537S MCF-7 cells stably expressing the ERE-NLuc reporter construct (ERE-NLuc) treated with the indicated doses of Ful. Experiments were performed three times, and each condition was tested in triplicate. Significant differences in the effect of Ful between the parental and L370F ERα expressing ERE-NLuc MCF-7 cells (* indicates $p < 0.05$) and the Y537S ERE-NLuc MCF-7 cells (° indicates $p < 0.05$) were calculated using the Student's t-test. **C** Growth curve analyses in parental and CRISPR/CAS9 engineered L370F and Y537S MCF-7 cells treated with the indicated doses of Ful. Experiments were performed using the xCelligence RTCA system. Dose response curves were calculated at the maximum proliferation of each cell line. The compound effect is the difference between the normalized cell index (NCI) value in the treated samples and the NCI value in the untreated samples (control, CTR) at the time point when cells reach the maximal growth (i.e., confluency). Significant differences in the effect of Ful between the parental and L370F ERα expressing MCF-7 cells (* indicates $p < 0.05$) and the Y537S MCF-7 cells (° indicates $p < 0.05$) were calculated using the Student's t-test

Next, we stably transfected the nanoluciferase reporter construct (ERE-NLuc) into parental, L370F, and Y537S MCF-7 cells to create cell lines for studying wt and ERα variant transcriptional activity (i.e., MCF-7 ERE-NLuc cells), as previously described [41]. In these cell lines, dose-response analyses of Ful's ability to reduce basal ERα transcriptional activity were performed by administering varying doses of Ful (10^{-13}M to 10^{-5}M) for 24 h. As shown in Fig. 2B, the inhibitory effect of Ful on receptor transcriptional activity was significantly reduced in L370F and Y537S MCF-7 ERE-NLuc cells compared to parental MCF-7 ERE-NLuc cells.

Growth curve analyses were performed in parental, L370F, and Y537S MCF-7 cells to evaluate the antiproliferative effects of Ful. Each cell line was treated with different doses of Ful (10^{-11}M to 10^{-5}M), and the resulting dose-dependent effect was measured at the time point when the control for each cell line reached maximum growth. Figure 2C shows that the antiproliferative effect induced by Ful in parental MCF-7 cells was significantly diminished in L370F MCF-7 cells, particularly at high Ful doses, and was almost entirely abolished in Y537S MCF-7 cells, as previously reported [20].

Overall, these data corroborate the results obtained from stable HEK293 cells and demonstrate that the L370F mutation in ERα confers resistance to Ful-induced ERα degradation and reduces the inhibitory effect of this ET drug on receptor transcriptional activity and cell proliferation.

Evaluation of the proliferation rate of parental, L370F and Y573S MCF-7 cells in the presence and absence of E2

Next, we studied the proliferation rate of parental, L370F, and Y537S MCF-7 cells under normal growth conditions (10% FBS) and in the presence of E2-deprived serum (10% charcoal stripped (CS-FBS)) using the xCELLigence apparatus.

Under normal growth conditions, parental MCF-7 cells reached maximal growth later than both the L370F and Y537S MCF-7 cells (Fig. 3A), with Y537S MCF-7 cells exhibiting the fastest growth rate, as previously reported [20, 42]. Accordingly, L370F and Y537S MCF-7 cells displayed a significantly shorter doubling time compared to parental MCF-7 cells, with Y537S MCF-7 cells having the shortest doubling time among the tested lines (inset in Fig. 3A). When growth curve analyses were performed in the presence of E2-deprived serum (10% CS-FBS), we confirmed that the growth of Y537S MCF-7 cells was

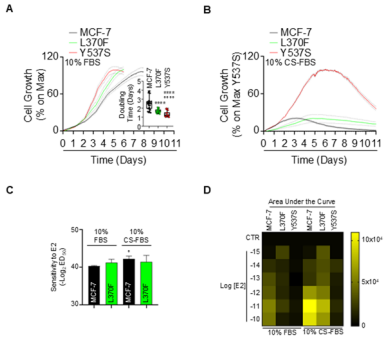

Fig. 3 Evaluation of the proliferation rate of the CRISPR/CAS9 engineered L370F MCF-7 cells. **A** Growth curve analyses in parental and CRISPR/CAS9 engineered L370F and Y537S MCF-7 cells plated in growing conditions (i.e., 10% FBS). Experiments were performed using the xCelligence RTCA system. Curves were calculated at the maximum proliferation of each cell line. (**inset in panel A**) Doubling time of the parental and the CRISPR/CAS9 engineered L370F and Y537S MCF-7 cells. Significant differences between the parental and the L370F or Y537S ERα expressing MCF-7 cells (**** indicates $p < 0.001$) and between the L370F and the Y537S MCF-7 cells (°°°° indicates $p < 0.001$) were calculated using the Student's t-test. Each dot indicates an experimental replicate. **B** Growth curve analyses in parental and CRISPR/CAS9 engineered L370F and Y537S MCF-7 cells plated in the presence of charcoal stripped fetal calf serum (i.e., 10% CS-FBS). Experiments were performed using the xCelligence RTCA system. Curves were calculated at the maximum proliferation of the CRISPR/CAS9 engineered Y537S MCF-7 cells. **C** The -Log_2 transformation of the effective concentration 50 (EC_{50}) of the 17β-estradiol (E2) effect in parental and L370F MCF-7 cells grown in the presence of either 10% FBS or 10% CS-FBS calculated at the time point where the most effective E2 dose curve reached the maximum. ° indicates the significant differences with respect to parental MCF-7 cells grown in 10% FBS were calculated using the Student's t-test ($p < 0.05$). **D** Heatmap showing the area under the curve (AUC) for each E2 treatment in each cell line grown in either 10% FBS or 10% CS-FBS. This panel has been generated using the data shown in Supplementary Fig. 2G and 2 H

E2-independent [20, 42] (Fig. 3B). Moreover, in contrast to parental MCF-7 cells, L370F MCF-7 cells did not exhibit reduced growth during prolonged E2 deprivation (Fig. 3B).

Next, we evaluated the proliferative effect of E2 in parental, L370F, and Y537S MCF-7 cells by administering various doses of E2 (from 10^{-15} M to 10^{-10} M) both under normal growth conditions (10% FBS) and in the presence of E2-deprived serum (10% CS-FBS) (Supplementary Fig. 2A-F). The sensitivity of parental and L370F MCF-7 cells to E2, calculated by -Log2 transforming the effective dose 50 (ED_{50}) for each cell line, was similar (Fig. 3C). Notably, as Y537S MCF-7 cell growth is E2-independent, the E2 ED_{50} in this cell line could not be extrapolated (Supplementary Fig. 2C and 2 F). Interestingly, parental MCF-7 cells grown in 10% CS-FBS show higher sensitivity to E2 compared to parental MCF-7 cells grown in 10% FBS (Fig. 3C).

To account for the time- and dose-dependent effects of E2 across all cell lines, we calculated the area under the curve (AUC) at each E2 dose in each cell line. We observed that in Y537S MCF-7 cells the AUC does not change as a function of E2 and is lower than that observed in parental MCF-7 cells, whereas in parental and L370F MCF-7 cells, E2 induces a dose-dependent variation in AUC (Fig. 3D and Supplementary Fig. 2G and 2 H). Interestingly, low doses of E2 generate a higher AUC in L370F MCF-7 cells than in parental cells, while high doses of E2 generate a lower AUC in L370F cells compared to parental cells (Fig. 3D and Supplementary Fig. 2G and 2 H). These data indicate that L370F MCF-7 cells respond to E2, with an enhanced effect at low doses and a reduced effect at high doses (Fig. 3D).

Overall, these results show that while Y537S cell growth is E2-independent, the proliferation of MCF-7 cells expressing the L370F ERα variant is partially E2-independent and can be stimulated by low E2 doses.

Analysis of E2-dependent regulation of ERα transcriptional functions in parental, and L370F MCF-7 cells

The parental and L370F MCF-7 ERE-NLuc cells were next used to evaluate the ability of E2 to modulate ERα transcriptional activity. A 24-hour administration of different doses of E2 (10^{-14}M to 10^{-8}M) revealed that the hormone induces a dose-dependent increase in ERα transcriptional activity in both cell lines (Fig. 4A). Notably, low-dose hormone treatment (10^{-13}M, 10^{-12}M) triggered a greater E2-dependent increase in receptor transcriptional activity in L370F MCF-7 ERE-NLuc cells compared to the parental MCF-7 ERE-NLuc line (Fig. 4A).

Phosphorylation of ERα at serine 118 (S118) is essential for its transcriptional activation in response to E2 [43]. E2-triggered ERα S118 phosphorylation occurs rapidly, reaching a maximum after 30 min of hormone administration in MCF-7 cells [43]. ERα S118 phosphorylation was evaluated in parental and L370F MCF-7 cells treated with different doses of E2 (10^{-14}M to 10^{-8}M) for 30 minutes. As shown in Fig. 4B and B', E2 dose-dependently increased the ERα S118 phosphorylation in both cell lines. However, the E2-induced receptor S118 phosphorylation was increased at low doses of the hormone (10^{-13}M to 10^{-10}M) in L370F MCF-7 cells with respect to the parental MCF-7 cells.

To confirm that the inhibitory effect of Ful on ERα transcriptional activity is reduced, and that E2-induced receptor transcriptional activity is increased at low hormone doses in L370F MCF-7 cells, we co-administered different doses of E2 and Ful for 24 h in both parental and L370F MCF-7 ERE-NLuc cells. The data revealed that antagonism between E2 and Ful was observed in both cell lines. However, the antagonistic interaction between E2 and Ful in L370F MCF-7 ERE-NLuc cells was significantly weaker as compared to parental MCF-7 ERE-NLuc cells (Fig. 4C). This indicates that Ful exhibits reduced antagonistic activity against E2 in regulating ERα

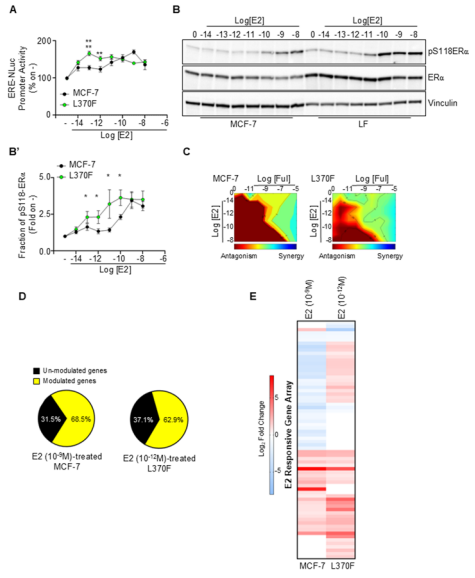

Fig. 4 Evaluation of the E2-dependent regulation of ERα transcriptional activity in CRISPR/CAS9 engineered L370F MCF-7 cells. **A** Dose-response of ERα transcriptional activity in parental and CRISPR/CAS9 engineered L370F MCF-7 ERE-NLuc cells plated in growing conditions (i.e., 10% FBS) treated with the indicated doses of 17β-estradiol (E2). Experiments were performed three times, and each condition was tested in triplicate. Significant differences in the effect of E2 between the parental and L370F MCF-7 ERE-NLuc cells were calculated using the Student's t-test (**** indicates $p < 0.0001$ and ** indicates $p < 0.01$). **B** Western blot and (**B'**) relative densitometric analyses of S118 phosphorylated and total ERα levels in parental and CRISPR/CAS9 engineered L370F MCF-7 cells treated for 30 min with the indicated doses of 17β-estradiol (E2). The experiment was performed in triplicate and significant differences in the effect of E2 between the parental and L370F ERα expressing MCF-7 cells were calculated using the Student's t-test (* indicates $p < 0.05$). **C** Antagonism (red) and synergy (blue) surfaces of ERα transcriptional activity in parental and CRISPR/CAS9 engineered L370F ERE-NLuc MCF-7 cells plated in growing conditions (i.e., 10% FBS) in the presence or in the absence of the co-treatment with 17β-estradiol (E2) (10^{-14}–10^{-8}M) and fulvestrant (Ful) (10^{-11}–10^{-5}M). Experiments were performed in duplicate. **D** Pie diagrams illustrating the percentages of modulated and un-modulated array genes in parental MCF-7 cells treated with 17β-estradiol (E2) (10^{-9}M) for 24 h and in CRISPR/CAS9 engineered L370F MCF-7 cells treated with E2 (10^{-12}M) for 24 h. Percentages and categories of genes are indicated. **E** Heatmap illustrating the E2-modulated genes between the parental MCF-7 cells treated with E2 (10^{-9}M) for 24 h and the CRISPR/CAS9 engineered L370F MCF-7 cells treated with E2 (10^{-12}M) for 24 h. Genes modulated by E2 < 0.7 and > 1.5 fold change with respect to untreated cells in each cell line were included in the analysis. Values are Log_2 transformed and used to generate the heatmap using the free online clustergrammer software (https://maayanlab.cloud/clustergrammer/)

transcriptional activity in L370F MCF-7 cells as compared to parental cells.

Since ERα regulates the expression of various genes, with or without the presence of ERE sequences in their promoter regions [44], we next assessed the E2 ability to modulate gene expression in parental and L370F MCF-7 cells. Based on previous data suggesting that the effect of E2 is enhanced in L370F MCF-7 cells treated with low E2 doses as compared to parental cells, we used an RT-qPCR-based array targeting 89 E2-sensitive genes [41]. We hybridized cDNA samples generated from total RNA extracted from parental MCF-7 cells treated with E2 at 10^{-9}M and from L370F MCF-7 cells treated with E2 at 10^{-12}M. Interestingly, despite the difference in concentration, E2 modulated most of the genes included in the array similarly in both parental and L370F MCF-7 cells (Fig. 4D), with a large overlap of genes regulated by E2 in both cell lines (Fig. 4E). Notably, for most of the genes commonly regulated by E2 at different doses, the E2 effect was larger in L370F MCF-7 cells than in parental cells (Fig. 4E and Supplementary Table 1). Overall, these data demonstrate that the L370F mutation renders ERα hypersensitive to low doses of E2, enhancing ERα transcriptional activity and E2-modulated gene expression.

Global gene expression profiling of ERα mutants reveals an increase in late E2 response gene in L370F MCF-7 cells

The data reported previously demonstrate that culturing the cells in E2-depleted medium allows the continuous growth of Y537S MCF-7 cells and causes a growth arrest in the L370F MCF-7 cells that is not followed by subsequent cell death, as it occurs in parental MCF-7 cells (Fig. 3B). Thus, to further evaluate the impact of the L370F ERα mutation in the regulation of E2 gene expression we performed RNA-seq analysis in parental, L370F and Y537S MCF-7 cells that had been maintained in E2-containing medium (i.e., normal growing condition – 10%-FBS) to identify changes in basal gene expression independent of the potential interferences caused by cell cycle-dependent regulation of gene expression.

We conducted RNA-seq analysis using three biological replicates for each cell line to estimate gene expression levels, measured as FPKM (Fragments Per Kilobase of transcript sequence per Million mapped reads) [45, 46]. Principal component analysis (PCA) of gene expression levels (FPKM) revealed strong clustering of biological replicates within each cell line, while both mutant lines (L370F and Y537S) showed clear separation from the parental MCF-7 cells (Supplementary Fig. 3 A). Furthermore, we calculated the correlation coefficients between samples across groups. A heatmap of these coefficients revealed high correlation within the biological replicates of each cell line (i.e., parental, L370F, and Y537S MCF-7 cells), indicating robust experimental consistency. Notably, parental and Y537S MCF-7 cells exhibited the lowest intergroup correlation coefficients, while the L370F MCF-7 cells showed an intermediate correlation, bridging both parental and Y537S profiles (Supplementary Fig. 3B).

The DESeq2 analysis (|log2(FoldChange)| >= 1 and padj < = 0.05) was performed to evaluate differential gene expression between L370F and parental MCF-7 cells, as well as Y537S and parental MCF-7 cells. This was

followed by generation of a ranked gene list in L370F (Supplementary Fig. 3C) and Y537S (Supplementary Fig. 3D) MCF-7 cells.

Initially, we analyzed the gene lists and observed that a substantial number of modulated genes were shared between L370F and Y537S MCF-7 cells (Supplementary Fig. 3E and Supplementary Table 2). Subsequently, we assessed whether the genes modulated in L370F and Y537S MCF-7 cells (relative to parental MCF-7 cells) with a signal-to-noise ratio > 0.5 or <−0.5 included both early and late E2-regulated genes (i.e., GSEA hallmark estrogen response early and hallmark estrogen response late gene sets [47]). Notably, the majority of early and late E2-regulated genes were modulated in L370F and Y537S MCF-7 cells (Fig. 5A and Supplementary Table 2) and a significant linear correlation (Spearman Correlation r = 0.47; $p < 0.0001$) was observed among the E2-regulated genes in L370F MCF-7 cells and in Y537S MCF-7 cells (Supplementary Fig. 3F). Cluster analysis (Fig. 5A and Supplementary Table 2) revealed groups of genes upregulated in both L370F and Y537S MCF-7 cells (e.g., RARα, and FASN) (Supplementary Fig. 3G and 3G'), specifically upregulated in Y537S cells (e.g., Cav-1 and FABP5) (Supplementary Fig. 3H and 3H') or in L370F cells (ASCL1 and CALCR) (Supplementary Fig. 3J and 3J'). Pathway enrichment analysis performed using genes belonging to clusters that differ between L370F and Y537S MCF-7 cells demonstrated that late estrogen genes are preferentially modulated in L370F MCF-7 cells (Fig. 5B) while early estrogen genes are preferentially modulated in Y537S cells (Fig. 5C).

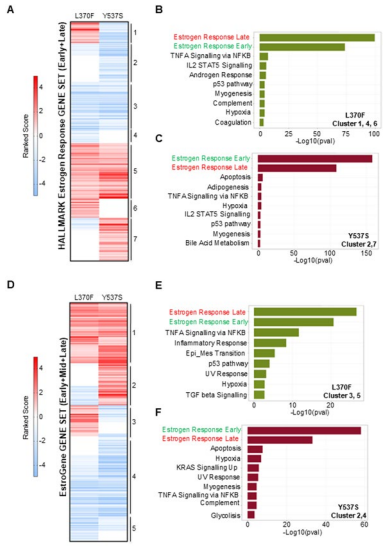

Fig. 5 Global gene expression analysis in parental and CRISPR/CAS9 engineered L370F and Y537S MCF-7 cells. Heatmaps illustrate the raked score of the genes belonging to the Estrogen Response Gene Set (HALLMARK) (**A**) or to the EstroGene Gene Set (**D**) found in the differential gene expression lists between L370F and parental MCF-7 cells (L370F) as well as Y537S and parental MCF-7 cells (Y537S). The heatmaps were generated using the free online clustergrammer software (https://maayanlab.cloud/clustergrammer/). **B**, **C** Pathway enrichment analyses of genes in the indicated clusters identified in Estrogen Response Gene Set (HALLMARK) for L370F and Y537S MCF-7 cells. (**E, F**) Pathway enrichment analyses of genes in the indicated clusters identified in EstroGene Gene Set for L370F and Y537S MCF-7 cells. Enrichment analyses were conducted using the free online easyGSEA software (https://tau.cmmt.ubc.ca/eVITTA/easyGSEA/)

Recently, the EstroGene database established robust signatures for basal and time-dependent E2 modulated genes (i.e., E2 response signature and early, mid, and late E2 response signatures) [48]. Therefore, we additionally analyzed our transcriptomic data using these gene sets. Also in this case, the majority of genes in the EstroGene signatures were modulated in L370F and Y537S MCF-7 cells (Supplementary Fig. 4A-D and Supplementary Table 2) and a significant linear correlation was observed among the EstroGene signature genes in L370F MCF-7 cells and in Y537S MCF-7 cells (Supplementary Fig. 4E-H). Cluster analysis of the early, mid and late E2 response signatures (Fig. 5D and Supplementary Table 2) followed by pathway enrichment performed using modulated genes belonging to clusters that differ between L370F and Y537S MCF-7 cells revealed also in this case that the L370F mutation preferentially regulates late estrogen response genes (Fig. 5E) while the Y537S mutation preferentially modulated early estrogen genes (Fig. 5F).

Finally, the DESeq2 analysis was performed to directly evaluate differential gene expression between L370F and Y537S MCF-7 cells performing pathway enrichment analyses using the first 5000 ranked genes in L370F (red dots in Fig. 6A) and in Y537S MCF-7 cells (blue dots in Fig. 6A). Figure 6B and C show that using the HALLMARK database late estrogen response genes were preferentially modulated in L370F MCF-7 cells with respect to Y537S MCF-7 cells while early estrogen response genes were enriched in Y537S MCF-7 cells with respect to L370F cells. Interestingly, pathway enrichment analysis using the Reactome database indicated that L370F MCF-7 cells significantly modulate energy metabolism (e.g., fatty acid metabolism) with respect to Y537S cells (Fig. 6D) and that Y537S MCF-7 cells significantly modulate translation metabolism with respect to L370F cells (Fig. 6E).

Altogether, these data (i) indicate that the basal regulation of E2-responsive genes in L370F MCF-7 cells closely resembles that observed in Y537S MCF-7 cells, thus suggesting that the introduction of the L370F mutation in ERα may enhance the activity of the mutant receptor compared to the wt ERα, particularly with respect to E2-sensitive genes and (ii) demonstrate that the L370F ERα variant preferentially modulates the expression of late E2-responsive genes.

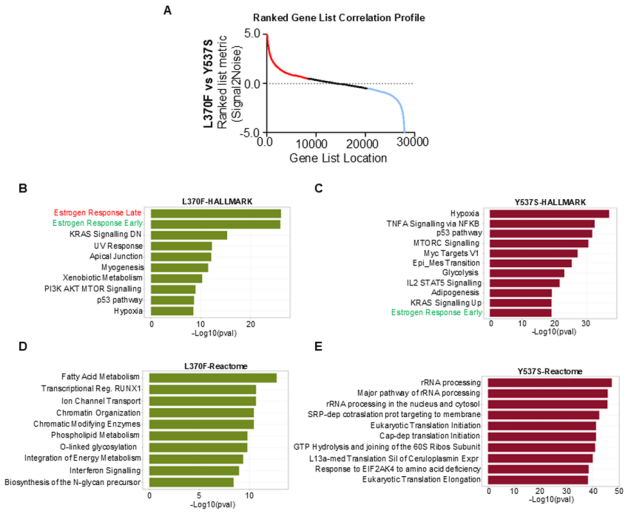

Fig. 6 Differential gene expression analysis in parental and CRISPR/CAS9 engineered L370F and Y537S MCF-7 cells. **A** Ranked gene list correlation profile of CRISPR/CAS9 engineered L370F MCF-7 cells with respect to Y537S MCF-7 cells. Pathway enrichment analyses of the first 5000 genes in the differentially modulated in L370F cells (red dots in panel A) or in Y537S MCF-7 cells (blue dots in panel A) using HALLMARK gene sets (**B**, **C**) or Reactome pathways (**D**, **E**). Enrichment analyses were conducted using the free online easyGSEA software (https://tau.cmmt.ubc.ca/eVITTA/easyGSEA/)

Table 1 Measurement of binding affinity towards full-length ERα

Recombinant full-lengh ERα	K_i (E2 - nM)	K_i (Ful - nM)
Wild type (from Thermo Scientific)	2.3 ± 0.9	4.8 ± 1.8
Wild type (purified in the present work)	1.6 ± 0.7	5.7 ± 2.1
L370F (purified in the present work)	4.0 ± 1.9 *	19.9 ± 6.7 **
Y537S (Purified in the present work)	24.3 ± 8.4 ***,°°°	30.3 ± 9.8 ***

The K_i for 17β-estradiol (E2) and fulvestrant (Ful) have been measured towards both the commercially available wild type ERα purified from insect cells (Thermo Scientific) and the wild type, L370F and Y537S full-length ERα purified from Epi293F cell lysates as described in the Material and Method section . Data are the mean ± the standard deviation of two independent experiments where each condition has been tested in quadruplicate

Significant differences were calculated using the Student's t-test

*, ** and *** indicates $p<0.05$, $p<0.01$ and $p<0.001$ with respect to the wild type ERα (purified in the present work), respectively. °°° indicates $p<0.001$ with respect to the L370F ERα (purified in the present work)

The impact of the L370F mutation on ERα ligand binding and on receptor structure

The biological effects of the L370F ERα mutation may be due to a reduced or impaired binding of agonist (E2) or antagonist (Ful) to ERα. To assess the binding affinities of E2 and Ful to the L370F ERα, we transiently expressed full-length wt, L370F, and Y537S ERα with a twin-strep tag in Epi293F cells and purified them using affinity chromatography. The resulting recombinant full-length wt, L370F, and Y537S ERα were then included in fluorescence polarization competitive binding assays, as previously described [14]. As additional control, we incorporated a commercially available wt ERα (Thermo Scientific), purified from insect cells, into our experimental plan.

Both E2 and Ful displaced the fluorescent E2 tracer across all tested receptors (Table 1). Notably, no significant differences were observed in the K_i values for E2 and Ful between the commercially available wt ERα and the recombinant wt ERα purified from Epi293F cells (relative binding affinity for E2 (RBA_{E2}) = 0.78 ± 0.42; RBA_{Ful} = 0.93 ± 0.45). However, as expected [40], the K_i of the Y537S mutant ERα for both E2 and Ful was significantly higher than that of the wt ERα (Table 1) (RBA_{E2} = 0.072 ± 0.036; RBA_{Ful} = 0.20 ± 0.09).

Interestingly, while the K_i of the L370F mutant ERα for E2 slightly increased with respect to that of the wt ERα, its absolute value remained within the same low nanomolar range (Table 1) (RBA_{E2} = 0.48 ± 0.30). In contrast, the K_i of the L370F mutant ERα for Ful was significantly higher than that of the wt ERα (Table 1) (RBA_{Ful} = 0.31 ± 0.14), and no significant differences were detected between the K_i values of the L370F and Y537S mutants for Ful (Table 1) (RBA_{Ful} = 0.71 ± 0.30).

These findings confirm that the Y537S mutation reduces the receptor's affinity for both E2 and Ful [40]. Notably they also reveal that while L370F mutation has only a minor impact on E2 binding to ERα, while it instead significantly reduces ERα's affinity for Ful.

Because we observed a reduction in Ful binding affinity towards the L370F receptor, we next performed classical molecular dynamics simulations to understand if the introduction of this mutation could alter the receptor structure, as observed for the Y537S ERα mutant. As shown in Fig. 7A and F, the L370F and to lower extend also E471D mutations result in a remodeling of helix H3 as compared to the wt ERα and to an ERα crystal structure in the antagonist conformation (pdb id:3ert [49]). In addition, the loop connecting H11 and H12 undergoes remodeling and moves closer to H3, leading to a partial disruption of H11's secondary structure. Consistently, with the above findings this behavior is more pronounced in the L370F mutant.

Aiming to inspect how the mutation affect the internal dynamical coupling of the receptor thus making it less sensitive to Ful, we then calculated the cross correlation coupling among the different ERα structural element, as done in previous studies [50] (Supplementary Fig. 5). Remarkably, the sum of correlation coefficients of H12 with H5 is higher than 4 only in the L370F mutant (Fig. 7G). This was previously considered as the threshold for the ERα activation in the previous study [18]. While the hydrogen bond network does not change significantly in any of the simulations, Ful shows less persistent hydrogen bonds with ERα in the mutant receptors than in the wt (Supplementary Tables 3–5).

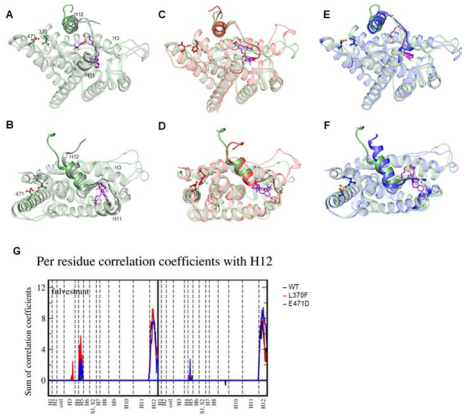

Fig. 7 Structural profile of wt and ERα L370F variant. Highest populated clusters of ERα (wt – gray, L370F – red, E471D – blue) from the equilibrated part of the trajectory superimposed on the 3ert crystal structure (green) (pdb id:3ert [49]), wt side view (**A**), wt top view (**B**), L370F side view (**C**), L370F top view (**D**), E471D side view (**E**), and E471D top view (**F**). Residues 370 and 471 are shown in balls and stick representation in the corresponding colour scheme of the protein and fulvestrant is depicted in violet. Helices H3, H11, and H12 are marked. **G** Sum of cross-correlation coefficients for interactions of residues with H12, monomer A is shown on the left and monomer B on the right side of the plot

Altogether these data indicate that the L370F mutation remodels ERα, reducing its affinity to Ful.

Evaluation of the ATRA antiproliferative effects in parental, L370F and Y537S MCF-7 cells

Previous data showed that L370F and Y537S MCF-7 cells express higher levels of RARα compared to parental MCF-7 cells (Supplementary Fig. 3G, and 3G'). Given that ATRA is a known antiproliferative agent for BC cells [51] and no information is available regarding its effects on cell lines expressing ERα point mutations found in MBC, we investigated the impact of this FDA-approved drug.

Growth curve analyses were performed on parental, L370F, and Y537S MCF-7 cells treated with varying doses of ATRA (10^{-10}M to 10^{-4}M). As expected [51], a 7-day ATRA treatment reduced the proliferation rate in all tested cell lines in a dose-dependent manner (Fig. 8A and C).

Interestingly, during the first 3–4 days of treatment, the normalized cell index (CI) measured using the xCELLigence system showed a transient increase in all cell lines, which was most pronounced in L370F MCF-7 cells (Fig. 8A-C). This increase was not due to enhanced proliferation but was instead attributable to ATRA-induced enlargement of the cellular surface, a feature accurately detected by the xCELLigence apparatus (Supplementary Fig. 6 A and 6A').

IC_{50} calculations revealed notable differences among the cell lines: L370F MCF-7 cells displayed the lowest IC_{50} value (16.2 ± 0.62 nM), parental MCF-7 cells

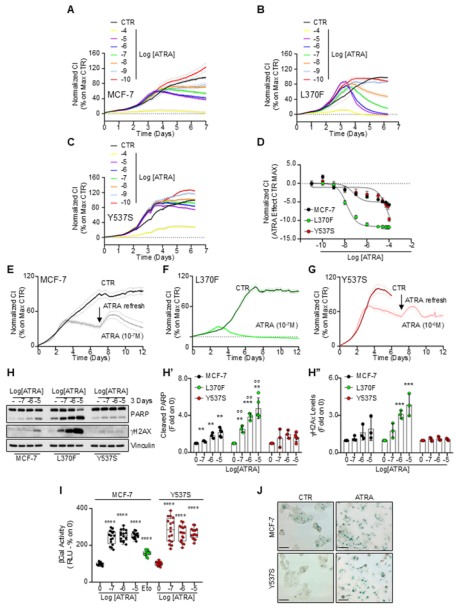

Fig. 8 The effect of ATRA in parental and CRISPR/CAS9 engineered L370F and Y537S MCF-7 cells. Growth curve analyses in parental (**A**), CRISPR/CAS9 engineered L370F (**B**) and Y537S (**C**) MCF-7 cells plated in growing conditions (i.e., 10% FBS) and treated with the indicated doses of all-trans retinoic acid (ATRA) for the indicated time. Experiments were performed using the xCelligence RTCA system. Curves were calculated at the maximum proliferation the untreated sample (control, CTR) in each cell line. **D** Dose response curves of ATRA effect were calculated at the maximum proliferation of the control sample (CTR). The effect of ATRA is the difference between the normalized cell index (NCI) value in the untreated samples and the NCI value in the treated samples at the time point when cells reach the maximal growth (i.e., confluency). Growth curve analyses in parental (**E**), CRISPR/CAS9 engineered L370F (**F**) and Y537S (**G**) MCF-7 cells plated in growing conditions (i.e., 10% FBS) and treated with the indicated doses of all-trans retinoic acid (ATRA) for the indicated time. Arrows indicate the time point where the medium was changed and ATRA administration was repeated. Experiments were performed using the xCelligence RTCA system. Curves were calculated at the maximum proliferation of the untreated sample (control – CTR) in each cell line. **H** Western blot and (**H' and H"**) relative densitometric analyses of PARP and phosphorylated γH2AX levels in parental, and CRISPR/CAS9 engineered L370F and Y537S MCF-7 cells treated for 3 days with the indicated doses of ATRA. Each dot indicates an experimental replicate. Significant differences in the effect of ATRA were calculated using the Student's t-test. ** ($p < 0.01$) and *** ($p < 0.001$) indicates differences with respect the untreated (0) sample in each cell line while °° ($p < 0.01$) indicates differences between the corresponding sample in parental MCF-7 cells. **I** Measurement of β-galactosidase activity (βGal) in parental and in CRISPR/CAS9 engineered Y537S MCF-7 cells treated with the indicated doses of ATRA for 12 days. As positive control parental MCF-7 cells were treated with etoposide (Eto 12.5 μM) and allowed to recover for 4 days. Each dot indicates an experimental replicate. Significant differences in the effect of ATRA were calculated using the Student's t-test. **** ($p < 0.0001$) indicates differences with respect to the untreated (0) sample in each cell line. (**J**) β-Galactosidase staining at pH 6.0 on parental and on CRISPR/CAS9 engineered Y537S MCF-7 cells treated with ATRA (10^{-7}M for MCF-7 cells and 10^{-6}M for Y537S MCF-7 cells) for 12 days. Scale bar = 100 μm

showed an intermediate value (91.2 ± 32.0 nM), and Y537S MCF-7 cells exhibited the highest IC_{50} (5.2 ± 3.9 μM) (Fig. 8D) and the antiproliferative maximal effect of ATRA was significantly greater in L370F MCF-7 cells compared to both parental and Y537S MCF-7 cells (Fig. 8D). Moreover, ATRA rapidly reduced the proliferation rate in L370F MCF-7 cells within 4–6 days, whereas the reduction in parental and Y537S MCF-7 cells over the same timeframe was slower (Fig. 8A and C). These findings suggest that ATRA exerts distinct antiproliferative effects across the different cell lines.

To explore this hypothesis, we extended the growth curve analyses to 12 days, monitoring proliferation in each cell line treated with the indicated doses of ATRA. Consistent with previous results, ATRA exhibited the strongest antiproliferative effect in L370F MCF-7 cells, the weakest in Y537S MCF-7 cells, and an intermediate effect in parental MCF-7 cells (Fig. 8E and G). Interestingly, L370F MCF-7 cells failed to proliferate entirely in the presence of ATRA (Fig. 8F). In contrast, parental and Y537S MCF-7 cells maintained their control-level proliferation rates for the first 2–3 days of ATRA treatment but then plateaued, sustaining an almost constant cell number over the remaining 9–10 days of the assay (Fig. 8E, and G).

These findings confirm the antiproliferative effect of ATRA on BC cells and demonstrate that its magnitude varies depending on the ERα variant expressed. Moreover, the results suggest that ATRA induces distinct cellular responses: cell death in L370F MCF-7 cells and a senescent-like phenotype in parental and Y537S MCF-7 cells.

To assess cell death, we next examined the ability of ATRA to induce PARP cleavage. Parental, L370F, and Y537S MCF-7 cells were treated with different doses of ATRA (10^{-7}M to 10^{-5}M) for 3 days. Western blotting analysis revealed that ATRA induced a significant and dose-dependent increase in PARP cleavage in L370F MCF-7 cells, whereas the effect was only marginal in parental and Y537S MCF-7 cells (Fig. 8H, upper panels and Fig. 8H'). Since it has been reported that ATRA could induce DNA damage in BC [52], which is closely linked to the initiation of cell death, we further evaluated its effect on the phosphorylation of histone H2AX (γH2AX), a well-established marker of DNA double-strand breaks [53]. As shown in Fig. 8H and H", ATRA administration for 3 days caused a robust and significant increase in γH2AX levels in L370F MCF-7 cells, while only a minor and not significant effect was observed in parental and Y537S MCF-7 cells. To understand the type of cell death induced by ATRA in L370F MCF-7 cells, annexin V exposure, caspase 3/7, caspase 8 and caspase 9 activities and necrosis was measured at different time points in L370F MCF-7 cells treated with ATRA. However, ATRA did not induce annexin V exposure (Supplementary Fig. 6B), caspase 3/7, caspase 8 and caspase 9 activation (Supplementary Fig. 6C) or necrotic cell death (Supplementary Fig. 6D). Because these data suggest ATRA induces a non-apoptotic cell death, the ATRA-induced antiproliferative effect was tested in L370F MCF-7 in the presence of the inhibitors of pyroptosis (disulfiram), ferroptosis (ferrostatin), necroptosis (necrostatin), and autophagy (bafilomycin A1). As shown in Supplementary Fig. 6E, none of these inhibitors were able to rescue the ATRA-induced reduction in cell proliferation, thus suggesting the exposure of L370F MCF-7 cells to ATRA induces atypical caspase-independent cell death.

To investigate the senescence-inducing potential of ATRA [52], parental and Y537S MCF-7 cells were treated with the indicated doses of ATRA for 12 days, after which the activation of the senescence associated β-galactosidase (SA-βGal) activity, a classical marker of senescence [54], was evaluated. As a positive control, etoposide was used to induce senescence in parental MCF-7 cells [55]. Figure 8I and J demonstrate that ATRA induced SA-βGal enzymatic activity in a dose-dependent manner in both cell lines, further confirming the onset of a senescent phenotype. As expected, ATRA was not able to induce SA-βGal activity in L370F MCF-7 cells (Supplementary Fig. 6F).

These findings collectively demonstrate that ATRA exerts differential effects on MCF-7 cell lines depending on the ERα variant expressed. Specifically, ATRA triggers non-apoptotic cell death in L370F MCF-7 cells, while it induces senescence in both parental and Y537S MCF-7 cells.

Evaluation of the RARα and ERα crosstalk in parental, L370F and Y537S MCF-7 cells

Since previous studies have demonstrated that ATRA and E2 signaling transcriptionally antagonize each other in BC cells [56], we hypothesized that the effects of ATRA in promoting non apoptotic cell death in L370F MCF-7 cells may be attributed to differences in the reciprocal regulation of RARα and ERα expression across parental, L370F, and Y537S MCF-7 cell lines.

To test this hypothesis, we assessed whether siRNA-induced depletion of either RARα or ERα differentially influenced the expression of ERα and RARα, respectively. Seventy-two hours after transfecting cells with siRNAs targeting RARα or ERα, the expression levels of both receptors were measured in parental, L370F, and Y537S MCF-7 cells. As expected, RARα-targeting siRNA reduced RARα expression, and ERα-targeting siRNA reduced ERα expression across all cell lines (Supplementary Fig. 7A, 7A' and 7A"). Notably, RARα depletion similarly affected ERα expression in all cell lines, and ERα depletion reciprocally reduced RARα expression to a

comparable extent in parental, L370F, and Y537S MCF-7 cells (Supplementary Fig. 7 A, 7A' and 7A"). In addition, we assessed the ability of ERα and RARα to be incorporated into the same molecular protein complex [57]. Stable HEK293 cell lines expressing HA- and His-tagged wt, L370F, and Y537S ERα were transiently transfected with flag-tagged RARα and subsequently subjected to Nickel (Ni) bead-based purification of ERα from total cellular lysates, followed by anti-flag WB analysis. As shown in Supplementary Fig. 7B-7D, wt, L370F, and Y537S ERα equally precipitated RARα. These findings confirm a regulatory crosstalk between RARα and ERα in BC cells and demonstrate that the introduction of the L370F and Y537S mutations in the ERα does not alter the mutual influence these receptors exert on each other's expression and interaction.

Next, we investigated the effects of ATRA on the expression levels of both ERα and RARα in parental, L370F, and Y537S MCF-7 cells. Cells were treated with increasing concentrations of ATRA (10^{-7}M to 10^{-5}M) for 72 hours, and receptor levels were assessed via WB analysis. As shown in Fig. 9A and A', ATRA induced a dose-dependent reduction in ERα expression in all three cell lines, with the effect being most pronounced in Y537S MCF-7 cells.

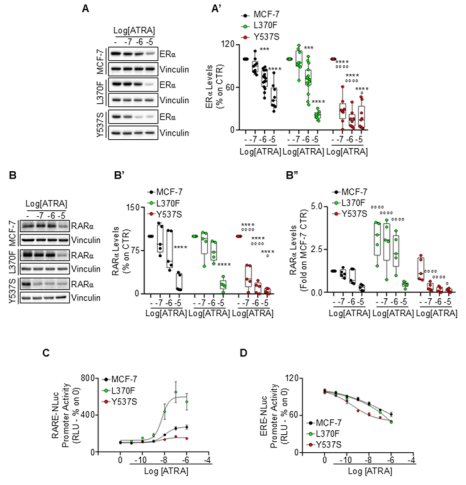

Fig. 9 ATRA-dependent regulation of RARα and ERα expression and transcriptional activity in parental and CRISPR/CAS9 engineered L370F and Y537S MCF-7 cells. **A** Western blot and (**A'**) relative densitometric analyses of ERα levels in parental and CRISPR/CAS9 engineered L370F and Y537S MCF-7 cells treated for 72 h with the indicated doses of all-trans retinoic acid (ATRA). Each dot indicates an experimental replicate. Significant differences in the effect of ATRA were calculated using the Student's t-test. *** and **** indicates $p < 0.001$ and $p < 0.0001$ with respect to control (-) samples. ° and °°°° indicates $p < 0.05$ and $p < 0.0001$ with respect to the corresponding samples in parental MCF-7 cells. **B** Western blot and (**B' and B"**) relative densitometric analyses of RARα levels in parental and CRISPR/CAS9 engineered L370F and Y537S MCF-7 cells treated for 72 h with the indicated doses of ATRA. Each dot indicates an experimental replicate. Significant differences in the effect of ATRA were calculated using the Student's t-test. **** indicates $p < 0.0001$ with respect to control (-) samples. ° and °°°° indicates $p < 0.05$ and $p < 0.0001$ with respect to the corresponding samples in parental MCF-7 cells. Dose-response of RARα transcriptional activity (**C**) and ERα transcriptional activity (**D**) in parental and CRISPR/CAS9 engineered L370F and Y537S MCF-7 cells stably expressing the RARE-NLuc reporter construct (NLuc) or the ERE-NLuc reporter construct (NLuc), respectively, treated with the indicated doses of ATRA. Experiments were performed three times, and each condition was tested in triplicate

In contrast, ATRA induced a dose-dependent decrease in RARα expression in Y537S MCF-7 cells, showing the greatest reduction among the three cell lines. However, only the highest dose (10^{-5}M) resulted in a significant decrease in RARα levels in parental and L370F MCF-7 cells (Fig. 9B and B'). Interestingly, baseline RARα expression levels were elevated in both L370F and Y537S MCF-7 cells compared to parental MCF-7 cells (control samples). However, ATRA treatment reduced RARα levels in Y537S MCF-7 cells below those of parental cells, while RARα levels in L370F MCF-7 cells remained higher than in parental cells (Fig. 9B and B").

Prompted by these observations, we hypothesized that ATRA-induced RARα activity might differ among parental, L370F, and Y537S MCF-7 cells. To test this, we generated stable cell lines expressing a reporter construct containing the retinoic acid receptor response element (RARE) fused to the nanoluciferase gene (RARE-NLuc). These cells were treated with ATRA at varying concentrations (10^{-11}M to 10^{-6}M) for 24 h to evaluate RARα transcriptional activity. ATRA dose-dependently increased RARα transcriptional activity in all cell lines (Fig. 9C). However, the response was highest in L370F MCF-7 RARE-NLuc cells and lowest in Y537S MCF-7 RARE-NLuc cells compared to parental cells.

Because ATRA reduced ERα expression in these cell lines and ERα degradation is intrinsically linked to the activation of ERα transcriptional activity [58, 59], we further assessed ATRA's impact on ERα transcriptional activity using parental, L370F, and Y537S MCF-7 ERE-NLuc cells. ATRA administration for 24 h caused a dose-dependent reduction in ERα transcriptional activity in all three cell lines, with the strongest effect observed in Y537S MCF-7 ERE-NLuc cells (Fig. 9D).

These findings indicate that ATRA-induced RARα transcriptional activity differs significantly in L370F and Y537S MCF-7 cells compared to parental cells. Notably, the ATRA-induced effects on RARα transcriptional activity (Fig. 9C) closely parallel the drug's antiproliferative effects in these cell lines (Fig. 8D), suggesting that the enhanced antiproliferative effect of ATRA in L370F MCF-7 cells may result from hyperactivation of RARα transcriptional activity.

Evaluation of the effect of digoxin on ATRA-induced senescence in parental, and Y537S MCF-7 cells

The induction of a senescent phenotype in cancer cells by therapeutic agents provides an opportunity to explore

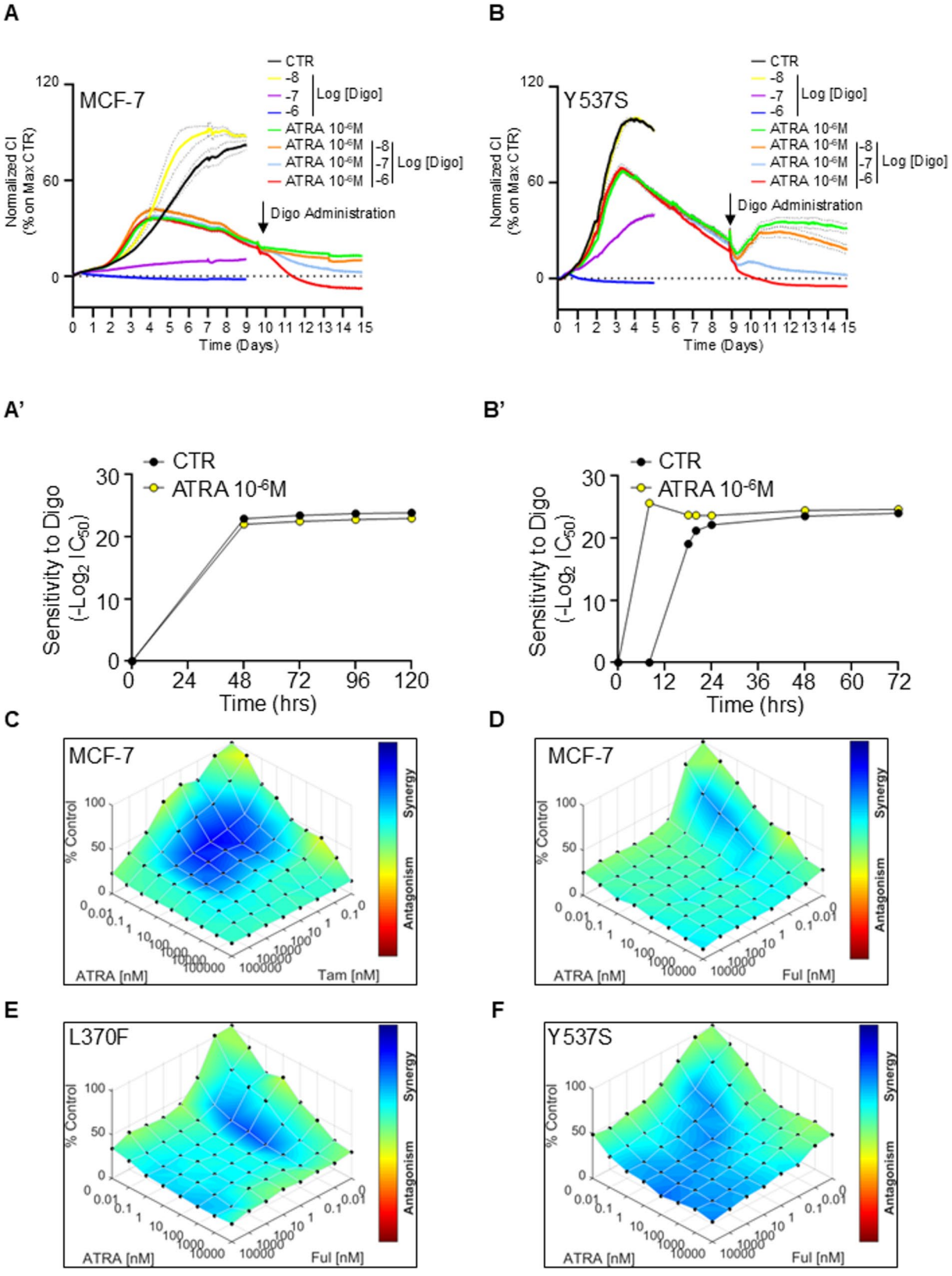

Fig. 10 (See legend on next page.)

(See figure on previous page.)

Fig. 10 The senolytic activity of digoxin in parental and CRISPR/CAS9 engineered L370F and Y537S MCF-7 cells. Growth curve analyses in parental (**A**), and in CRISPR/CAS9 engineered Y537S (**B**) MCF-7 cells plated in growing conditions (i.e., 10% FBS) and treated with the indicated doses of all-trans retinoic acid (ATRA) or digoxin (Digo) for the indicated time. Black arrows indicate the time point in which media was changed and ATRA was re-administered together with the indicated doses of Digo and the proliferation profile was followed up to 15 days. Experiments were performed twice in duplicate using the xCelligence RTCA system. Curves were calculated at the maximum proliferation the untreated sample in each cell line. **A** Time dependent inhibitory concentration 50 (IC_{50}) -Log_2 transformed to indicate the sensitivity of parental (**A'**) and CRISPR/CAS9 engineered Y537S (**B'**) MCF-7 cells to Digo both in the absence (CTR) and in the presence of the indicated dose of ATRA. **C** Synergy map of 12-day-treated parental MCF-7 cells with different doses of 4OH-Tamoxifen (Tam) and ATRA. **D** Synergy map of 10-day-treated MCF-7 cells with different doses of fulvestrant (Ful) and ATRA. **E** Synergy map of 5-day-treated L370F MCF-7 cells with different doses of fulvestrant (Ful) and ATRA. **F** Synergy map of 4-day-treated Y537S MCF-7 cells with different doses of fulvestrant (Ful) and ATRA

novel anticancer strategies, such as using compounds that selectively eliminate senescent cells (i.e., senolytics) [60]. Therefore, we investigated the potential of digoxin (Digo), an FDA-approved cardiac glycoside with known senolytic activity [61], to target ATRA-induced senescent parental and Y537S MCF-7 cells. To this end, we performed growth curve analyses on parental and Y537S MCF-7 cells treated with various concentrations of Digo (10^{-8}M to 10^{-6}M) both in the absence and presence of ATRA (10^{-6}M). As expected, Digo induced a dose-dependent reduction in the proliferation rate of both parental and Y537S MCF-7 cells. Similarly, ATRA (10^{-6}M) consistently reduced the proliferation of these cell lines over time (Fig. 10A and B). Following 10 days of continuous ATRA administration, when senescence was previously confirmed (Fig. 8), we introduced different doses of Digo (10^{-8}M to 10^{-6}M) to the parental and Y537S MCF-7 cells and monitored their proliferation rates over an additional 5-day period. Under these conditions, Digo again caused a dose-dependent decrease in the proliferation rate of both cell lines (Fig. 10A and B).

To quantitatively assess the effect of Digo, we calculated its IC_{50} values at different time points after administration, both in the absence and presence of ATRA. The IC_{50} values were mathematically transformed (i.e., -Log_2) to evaluate the sensitivity of both cell lines to Digo. The overall sensitivity to Digo was similar in both cell lines both in the absence and presence of ATRA (Fig. 10A' and 10B'). However, while the parental MCF-7 cells exhibited no significant differences in Digo sensitivity over time, regardless of ATRA treatment (Fig. 10A'), Y537S MCF-7 cells showed enhanced sensitivity to Digo in the presence of ATRA compared to its absence (Fig. 10B').

These findings demonstrate that the antiproliferative effect of Digo during prolonged ATRA treatment manifests more rapidly in Y537S MCF-7 cells compared to parental MCF-7 cells. This observation strongly suggests that Digo could function as a senolytic agent specifically in ATRA-induced senescent Y537S MCF-7 cells.

Finally, we investigated the combined effects of ATRA and Tam, a cornerstone therapy for patients with ERα-expressing primary BC [1], in parental MCF-7 cells and the combined effects of ATRA and Ful in parental, L370F and Y537S MCF-7 cells. The results demonstrated a synergistic interaction between ATRA and Tam in parental MCF-7 cells (Fig. 10C) and ATRA and Ful showed a range of synergy in all the tested cell lines (parental < L370F < Y537S MCF-7 cells) (Fig. 10D and F).

These findings suggest the potential use of ATRA in combination with Tam for the treatment of primary BC and in combination with Ful for the treatment of MBC expressing ERα mutations.

Discussion

The mainstay treatment for ERα-expressing primary breast cancer (BC) involves endocrine therapy (ET) with drugs such as aromatase inhibitors (AIs) and 4OH-tamoxifen (Tam). This treatment is typically administered for 5 to 10 years following diagnosis and has significantly reduced BC mortality rates. However, the extended duration of therapy often leads to the development of resistance to ET drugs in a substantial subset of patients, resulting in relapse and progression to metastatic breast cancer (MBC), which is frequently fatal [1].

Resistance to ET drugs arises through multiple mechanisms, including the selection of ERα point mutations in MBC cells that drive uncontrolled proliferation. Most of these ERα variants occur within the receptor's ligand-binding domain (LBD) and induce structural rearrangements that mimic the three-dimensional conformation of the wt receptor bound to E2. This constitutively active agonist conformation not only promotes continuous proliferative signaling but also renders the mutated receptor insensitive to anti-estrogen therapies, such as Ful [15, 40]. Targeting ERα point mutations in MBC is therefore crucial for developing strategies to manage the disease. Various therapeutic approaches, including SERDs, SERCAs, PROTACs, CERANs, and other targeted drugs [11–14], have been explored to inhibit the metastatic potential of mutant ERα variants. Promisingly, clinical trials have demonstrated the efficacy of some of these agents, such as elacestrant [6] and camizestrant [5, 7], in combating receptor mutations, leading to the approval of elacestrant and imlunestrant for clinical use [2, 6, 10].

Despite these advancements, preclinical and clinical studies have predominantly focused on the most frequent ERα mutations, such as Y537S, while neglecting the functional impact of less common ERα variants. These

lesser-studied mutations are equally associated with reduced patient survival and contribute to therapy resistance via variant-specific mechanisms [15]. For example, Irani et al. [16] reported that mutations in the ERα dimerization domain led to constitutive transcriptional activation, promoting cell proliferation. This study also proposed that disrupting receptor dimerization could serve as a novel therapeutic strategy for MBC [16].

These findings not only highlight the urgent need to characterize all ERα variants expressed in MBC to identify new therapeutic targets but also underscore the role of three-dimensional structural determinants in deregulating specific receptor functions (e.g., such as ERα dimerization, and nuclear localization), thus opening the possibility that specific neglected ERα variant could be treated with specific drugs.

L370F ERα mutation as a novel natural receptor variant conferring resistance to fulvestrant

We investigated two clinically observed ERα mutations, L370F and E471D, which are annotated in the COSMIC and cBioPortal databases. These mutations affect residues positioned across from each other on helices H4 and H10 within the ERα LBD, pointing to a potential new structural hotspot. To study the effect of these ERα mutations, we used both HEK293 cell lines overexpressing the receptors [38, 43, 62] and CRISPR/CAS9 engineered MCF-7 cells. HEK293 cells are ERα negative cell lines, which were previously used as a model where to stably insert the ERα because the resulting cell line responds to E2 like other endogenously expressing ERα cell lines (e.g., MCF-7 cells) and is useful to evaluate the impact of specific ERα mutations in E2:ERα signalling without the interference of the endogenous ERα [62]. MCF-7 cells instead were used to generate a pre-clinical cell model system that could mimic the presence of the L370F mutation in a cellular condition closer to the one found in tumor cells. Although we studied the effect of the L370F mutation only in one type of BC cell line and results would require additional validation in other relevant cellular contexts, MCF-7 cells are considered the gold standard model to study E2:ERα signaling and they have been previously used to characterize other receptor mutants found in MBC (e.g., Y537S ERα) [20, 42].

Using the combination of these two model systems together with in vitro and in silico studies, we demonstrate that the L370F and E471D mutations differently affect sensitivity to Ful. Specifically, the L370F variant reduces sensitivity to Ful. On the contrary, the E471D variant does not impair the ability of Ful to reduce both receptor transcriptional activity and ERα intracellular levels and it does not significantly change the LBD structure.

For these reasons, we decided to exclude the E471D mutation from additional analyses and further characterization of the L370F mutation revealed that it confers several distinct properties to BC cells such as (i) reduced sensitivity to Ful in terms of ERα transcriptional activity, receptor stability, and cell proliferation; (ii) hyperactive proliferation in response to low E2 doses; and (iii) basal upregulation of late E2 response genes.

The L370F ERα mutation effects on fulvestrant sensitivity, E2 signaling and cell proliferation

Our data show that the recombinant purified L370F receptor exhibits reduced binding affinity for Ful compared to the wt receptor. All atoms' simulations further confirmed this finding elucidating that the lower binding of Ful to this ERα variant is due to a structural reorganization of the H4-H5-H12 region in the ERα antagonist conformation. Altogether in vitro and in silico findings provide evidence that the natural mutation of ERα at residue L370 alters the receptor's structure, which impairs Ful binding, similarly to what observed for the Y537S ERα variant [40]. Notably, simulation analyses performed on the E471D mutant ERα revealed that this mutation has a minor effect on the receptor structure and Ful binding. On one hand, this result supports the lack of Ful effect on ERα transcriptional activity; on the other hand, it suggests that the different point mutations found in MBC patients could also affect three-dimensional structural clusters. This further opens the possibility that distant mutations (e.g., in domains other than the LBD) could influence the structure-function of the LBD, and in turn, antagonist binding and receptor cellular functions.

The L370F mutant structural remodeling and reduced binding affinity to Ful contribute to the diminished effect of Ful on the transcriptional activity, receptor degradation, and cell proliferation of the L370F ERα variant. In both stable HEK293 cells overexpressing the L370F ERα variant and L370F MCF-7 cells, we observed that this mutation attenuates the effect of Ful, particularly at high drug doses. These results demonstrate that the L370F ERα point mutation confers resistance to the ET drug Ful. Notably, this resistance is significant in the context of high-dose Ful administration (e.g., 500 mg/Kg), which has been shown to enhance anti-tumor effects in patients [1].

Growth curve analysis under 10% serum conditions revealed that cells expressing the L370F ERα variant have a reduced doubling time compared to wt ERα-expressing cells, and their proliferation rate is similar to that of Y537S MCF-7 cells. Interestingly, the growth behavior of L370F-expressing cells mirrors that of Y537S MCF-7 cells. Conversely, when grown in an E2-deprived medium, the Y537S MCF-7 cells continue to proliferate, while parental MCF-7 cells stop growing and eventually

die. In contrast, L370F MCF-7 cells cease growth but survive in the absence of E2. Upon E2 administration, parental MCF-7 cells remain sensitive to the hormone, while Y537S MCF-7 cells are unresponsive. However, L370F MCF-7 cells respond to E2 in terms of cell proliferation only when grown in an E2-deprived medium. In a medium containing E2, L370F MCF-7 cells exhibit only a minimal response to E2. Notably, at low E2 doses, the L370F ERα variant displays hyperactivity in terms of E2-dependent cell proliferation compared to the wt receptor. This effect is also evident in terms of receptor transcriptional activity. Although the specific mechanisms underlying this effect were not investigated, our in silico simulations of the L370F ERα suggest a structural reorganization of the receptor. This, combined with the similar binding affinity for E2 as observed in the wt ERα, could facilitate the response to E2. Alternatively, the differential sensitivity to E2 may result from the recruitment of distinct co-activators by the L370F mutant receptor compared to the wt ERα. Interestingly, the ability of the L370F ERα variant to respond to low E2 doses may support metastatic cell proliferation. Indeed, in menopausal women or those undergoing ovarian function inhibition, plasma E2 levels are in the picomolar range [63]. In this context, the L370F mutation activates key functions of the mutant receptor, suggesting that receptor activation at low E2 doses may represent a novel mechanism by which BC cells adapt to the hostile environment created by ET drugs (e.g., AI).

One hallmark of the Y537S mutation is the receptor's ability to constitutively modulate E2-regulated genes, independent of E2 binding [40]. Our transcriptomic analysis revealed that the Y537S and L370F ERα mutants regulate a similar number of genes, with several E2-sensitive genes being upregulated in both mutant cell lines. Interestingly, the extent of upregulation differed between the two cell lines, with some genes specifically upregulated in one line or the other. Moreover, our data showed that in Y537S MCF-7 cells, genes from both early and late E2 responses were upregulated, whereas in L370F MCF-7 cells, genes from the late E2 response class were more prominently upregulated. Thus, the overall E2 response differs between the two cell lines and may be due to the ability of the L370F ERα to associate with distinct chromatin regions compared to the Y537S variant. Future ChIP-Seq analyses are necessary to further elucidate these differences. However, the selective upregulation of late E2 response genes by the L370F ERα variant highlights its role in promoting cell cycle progression and supporting the development of resistance to ET drugs [64].

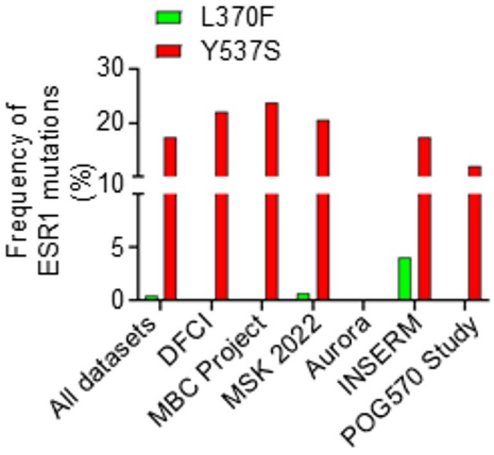

Fig. 11 The frequency of the L370F and Y537S *ESR1* mutations in metastatic breast cancer datasets. Frequency of the L370F and Y537S mutation has been extracted by the published studies and the cBioportal database. In particular, the used datasets were Dana Faber Cancer Institute (DFCI) [67]; INSERM [68]; AURORA US Network (AURORA) [69], POG570 study [70]; Metastatic Breast Cancer Project [https://mbcproject.org/] (MBC Projects) and Metastatic Breast Cancer - Memorial Sloan Kettering Cancer Discovery 2022 (MSK 2022) data were retrieved from cBioportal

The clinical relevance of the L370F ERα mutation in the context of the neglected ERα variants

It is important to clarify the potential clinical significance of the L370F ERα variant. Among annotated ERα mutations, some are frequently observed in patients, while others are rarer [65]. Regardless of their prevalence, these mutations generally exhibit poor responsiveness to existing therapies and negatively impact patient survival [65]. At the present, no information is available regarding the pool of patients who may be affected by the L370F ERα mutation, and calculating its frequency is challenging. However, based on literature data on BC epidemiology [66], it is possible to estimate the frequency of affected patients by using the data available in studies focusing only on metastatic breast cancer cohorts and excluding primary tumors, for the L370F mutation compared to the Y537S mutation (Fig. 11).

In these datasets (i.e., Dana Faber Cancer Institute [67]; INSERM [68]; the Metastatic Breast Cancer Project [https://mbcproject.org/] and Metastatic Breast Cancer - Memorial Sloan Kettering Cancer Discovery 2022 [cBioportal]; AURORA US Network [69], POG570 study [70]), 98 out of 568 patients are positive for the Y537S mutation (i.e., 17,25%) while only 3 out of 568 patients are positive for the L370F mutation (i.e., 5,28‰). Despite its rarity, our findings demonstrate that the L370F ERα mutation provides BC cells with selective advantages for metastatic growth. These findings highlight the need to investigate the biological impact of rare ERα mutations in MBC. Moreover, it is possible that some ERα mutations

are classified as rare simply because they are overlooked in current research and diagnostic efforts.

Currently, next-generation sequencing or droplet digital PCR experiments (ddPCR) are used to detect ERα mutations [71]. ddPCR is used to identify only known and most frequent ERα mutations (e.g., exon 5 to exon 8, i.e., ERα LBD) while other mutations and/or those located outside the LBD are not actively searched in patient samples, unless whole exome sequencing, an expensive and time consuming method [65], is performed. For example, no screening protocols exist for mutations located in the ERα A/B domain, and the L370F mutation located in exon 5 cannot be identified as the standard oligonucleotides used for ddPCR-based detection of that region contain the L370 wt codon [71]. This diagnostic bias neglects mutations that may significantly contribute to disease progression, as exemplified by the L370F ERα variant described herein, and others previously reported [16, 17]. This limitation is critical because no specific treatment protocols currently exist for MBC patients harboring these neglected ERα mutations, leaving these individuals without access to personalized therapy.

The increased sensitivity of the L370F ERα mutation to ATRA anti-proliferative effect

Interestingly, we observed that both L370F and Y537S MCF-7 cells express elevated levels of RARα. Using the EstroGene 2.0 database [72], analysis of gene expression changes across 46 comparisons between different cell lines expressing various *ESR1* mutations (i.e., S463P, E380Q, L536R, Y537S/N/C, and D538G) and their wt counterparts revealed, as expected, that the percentage of datasets in which the E2 target genes *TFF1*, *PRG*, and *CTDS* were up-regulated was higher than the percentage in which they were down-regulated (Supplementary Fig. 8). Interestingly, among the retinoic acid receptor family members (i.e., *RARA*, *RARB*, *RARG*, *RXRA*, *RXRB*, *RXRG*), only *RARA* showed a higher percentage of datasets with up-regulated expressions than with down-regulated expression (Supplementary Fig. 8). Therefore, *RARA* expression is up-regulated in several cell models expressing *ESR1* mutations (e.g., Y537S, D538G) and the increased RARα protein levels could be considered as a common feature of MBC expressing ERα-expressing variants.

These results prompted us to investigate the antiproliferative effects of ATRA in both L370F and Y537S MCF-7 cells [51]. In turn, we show that L370F ERα-expressing cells are more sensitive to ATRA than parental or Y537S MCF-7 cells. Importantly, ATRA triggers substantial DNA damage and pronounced cell death selectively in L370F cells. The cell death induced by ATRA in this cell line does not depend on caspase activation and does not induce annexin V exposure or a necrotic phenotype. Additionally, this ATRA-induced effect is not prevented by inhibitors of pyroptosis, ferroptosis, necroptosis, or autophagy. This pattern suggests that ATRA triggers a non-apoptotic atypical form of programmed cell death that is caspase independent. Further studies are required to determine the specific cell death pathway activated by ATRA in these cells.

Initially, we hypothesized that this effect might arise from an interaction between RARα and ERα [56]. However, the presence of the L370F and Y537S mutations did not alter the reciprocal regulation of receptor levels, their potential physical interaction with RARα or the ability of ATRA to activate RARα transcriptional activity and to inhibit ERα transcriptional activity. Furthermore, ATRA did not bind in vitro to wt, L370F and Y537S ERα (data not shown). Nevertheless, we found that ATRA-induced activation of RARα transcriptional activity is significantly enhanced in L370F cells. Given previous findings that R-loops generated during the E2 transcriptional response contribute to DNA damage and genomic instability in BC cells [73, 74], we speculate that ATRA-dependent hyperactivation of RARα transcription leads to transcriptional stress (e.g., R-loops), DNA damage, and subsequent cell death, thereby explaining the heightened sensitivity of L370F cells to ATRA.

Growth curve analyses and cellular assays revealed that ATRA induces senescence in parental and Y537S MCF-7 cells. While ATRA-induced senescence in BC cells has been previously reported [52], this is, to our knowledge, the first evidence of a drug inducing senescence in a BC cell line expressing the Y537S ERα variant. Exploiting senescence as a therapeutic strategy is increasingly recognized for its potential to overcome treatment resistance, as it creates vulnerabilities that can be targeted with senolytic agents in a 'one-two punch' approach [60]. Accordingly, we found that digoxin, an FDA-approved cardiac glycoside with known senolytic activity [61], selectively targets ATRA-induced senescence in Y537S MCF-7 cells but not in parental cells.

The clinical potential of ATRA has been demonstrated by its success in treating acute promyelocytic leukemia, inspiring efforts to explore its use in solid tumors [75, 76]. Although studies consistently report ATRA's inhibitory effects on BC cell growth, this knowledge has led to only a limited number of clinical trials investigating ATRA as an anti-BC agent [77]. Moreover, no data currently address the potential use of ATRA in treating MBC expressing ERα mutations. However, our findings highlight three potential applications of ATRA in BC clinical practice. First, we observed that co-administration of ATRA with Tam produces a synergistic antiproliferative effect in parental MCF-7 cells, indicating its potential use in managing primary ERα expressing BC that are suitable

for ET. Moreover, ATRA could also restores the sensitivity to Ful in MBC expressing the L370F and Y537S ERα variant, highlighting its potential use in drug combination protocols for the treatment of MBC. Additionally, ATRA could be implemented as a chemotherapeutic agent for treating MBC expressing the L370F ERα variant. Finally, ATRA could be employed to induce cellular senescence in MBC expressing the Y537S ERα variant, creating an opportunity for subsequent senolytic therapy.

Conclusions

This study identifies the L370F ERα mutation as a novel natural variant associated with MBC and elucidates the mechanisms through which it contributes to ET resistance and metastatic growth. Our findings highlight the importance of characterizing all ERα mutations, including those currently neglected, to better understand their roles in disease progression and therapy resistance. Furthermore, we provide evidence that different ERα variants exhibit unique sensitivities to specific drugs, such as ATRA, which can elicit distinct therapeutic effects depending on the mutation.

Overall, this work demonstrates that tailoring treatment based on the specific ERα variant expressed in MBC can pave the way for more effective and personalized BC therapies.

Abbreviations

AI	aromatase inhibitors
ASCL1	Achaete-Scute Family BHLH Transcription Factor 1
ATRA	All-trans retinoic acid
BC	Breast cancer
CALCR	Calcitonin Receptor
CDK4	Cyclin-dependent kinase 4
CDK6	Cyclin-dependent kinase 6
CERAN	Complete estrogen receptor antagonists
CS-FBS	Charcoal Stripped Fetal bovine serum
ddPCR	droplet digital PCR
Digo	Digoxin
E2	17β-estradiol
ERE	Estrogen responsive element
ERα	Estrogen receptor α
ET	Endocrine therapy
FABP5	Fatty acid binding protein 5
FASN	Fatty acid synthase
FBS	Fetal bovine serum
FDA	Food and Drug Administration
FPKN	Fragments Per Kilobase of transcript
Ful	Fulvestrant
HER2	Human Epidermal Growth Factor Receptor 2
LBD	Ligand binding domain
MBC	Metastatic breast cancer
NLuc	Nanoluciferase
PCA	Principal component analysis
PROTAC	Proteolysis targeting chimerics
RARE	Retinoic acid response element
RARα	Retinoic acid receptor α
SERCA	Selective estrogen receptor covalent antagonist
SERD	Selective estrogen receptor downmodulator
SERM	Selective estrogen receptor modulator
Tam	4OH-tamoxifen
WB	Western Blot
wt	wild type
γH2AX	phosphorylated H2A Histone Family Member X

Supplementary Information

The online version contains supplementary material available at https://doi.org/10.1186/s12964-025-02639-5.

Supplementary Material 1.

Supplementary Material 2.

Supplementary Material 3.

Supplementary Material 4.

Supplementary Material 5.

Acknowledgements

We thank A. Scardua and J. Weber (Biomass Production Unit, National Facility for Structural Biology, Human Technopole) for support and service provision. Access to National Facility was granted to Project ID 1771263. The authors are grateful to Prof. Simak Ali, University of London Imperial College for the gift of the MCF-7 Y537S cells. The anti-FASN antibody was a generous gift of Prof. Andrea Morandi, Dipartimento di Scienze Biomediche Sperimentali e Cliniche 'Mario Serio', Firenze, Italy.

Authors' contributions

M.C. performed most of the experimental work. C.B. performed transcriptional studies. M.F. performed measurements of cellular surface. M.P. and A.M. performed in silico studies. F.A. conceptualized the research, formally analyzed the data, wrote, reviewed, and edited the manuscript. All authors reviewed the manuscript.

Funding

The research leading to these results has received funding from AIRC under IG 2018 - ID. 21325 project – P.I. Acconcia Filippo. The Grant of Excellence Departments 2023–2027, MIUR (ARTICOLO 1, COMMI 314–337 LEGGE 232/2016) to the Department of Science, University Roma TRE is also gratefully acknowledged. This study was also supported by grants from Ministero della Salute RF-2021-12372851; CUPF83C22002620001 to Acconcia Filippo.

Data availability

Densitometric analyses of each WB, as well as original data for growth curves and synergy proliferation experiments, are available from the corresponding author on reasonable request. All the original Western blots are available in Supplementary Materials.

Declarations

Ethics approval and consent to participate

Not applicable.

Consent for publication

Not applicable.

Competing interests

The authors declare no competing interests.

Author details

[1]Department of Sciences, Section Biomedical Sciences and Technology, University Roma TRE, Rome, Italy
[2]Department of Chemical Reaction Engineering, National Institute of Chemistry, Hajdrihova 19, Ljubljana SI-1001, Slovenia
[3]National Research Council-Insitute of Material Foundry (CNR-IOM) at International School for Advanced Studies (SISSA/ISAS), via Bonomea 265, Trieste 34136, Italy

Received: 26 June 2025 / Accepted: 26 December 2025
Published online: 05 January 2026

References

1. Will M, Liang J, Metcalfe C, Chandarlapaty S. Therapeutic resistance to anti-oestrogen therapy in breast cancer. Nat Rev Cancer. 2023;23:673–85. https://doi.org/10.1038/s41568-023-00604-3.
2. Shah M, Lingam H, Gao X, Gittleman H, Fiero MH, Krol D, Biel N, Ricks TK, Fu W, Hamed S, Li F, Sun JJ, Fan J, Schuck R, Grimstein M, Tang L, Kalavar S, Abukhdeir A, Pathak A, Ghosh S, Bulatao I, Tilley A, Pierce WF, Mixter BD, Tang S, Pazdur R, Kluetz P, Amiri-Kordestani. L 2024 US food and drug administration approval summary: elacestrant for Estrogen receptor-Positive, human epidermal growth factor receptor 2-Negative, ESR1-Mutated advanced or metastatic breast cancer. J Clin Oncol:JCO2302112. https://doi.org/10.1200/JCO.23.02112.
3. Patel R, Klein P, Tiersten A, Sparano JA. An emerging generation of endocrine therapies in breast cancer: a clinical perspective. NPJ Breast Cancer. 2023;9:20. https://doi.org/10.1038/s41523-023-00523-4.
4. Shastry M, Hamilton E. Novel Estrogen Receptor-Targeted agents for breast cancer. Curr Treat Options Oncol. 2023;24:821–44. https://doi.org/10.1007/s11864-023-01079-y.
5. Oliveira M, Pominchuk D, Nowecki Z, Hamilton E, Kulyaba Y, Andabekov T, et al. Camizestrant, a next-generation oral SERD, versus fulvestrant in post-menopausal women with oestrogen receptor-positive, HER2-negative advanced breast cancer (SERENA-2): a multi-dose, open-label, randomised, phase 2 trial. Lancet Oncol. 2024;25:1424–39. https://doi.org/10.1016/S1470-2045(24)00387-5.
6. Bidard FC, Kaklamani VG, Neven P, Streich G, Montero AJ, Forget F, et al. Elacestrant (oral selective estrogen receptor degrader) versus standard endocrine therapy for estrogen receptor-positive, human epidermal growth factor receptor 2-negative advanced breast cancer: results from the randomized phase III EMERALD trial. J Clin Oncol. 2022;40:3246–56. https://doi.org/10.1200/JCO.22.00338.
7. Hamilton E, Oliveira M, Turner N, Garcia-Corbacho J, Hernando C, Ciruelos EM, et al. A phase I dose escalation and expansion trial of the next-generation oral SERD camizestrant in women with ER-positive, HER2-negative advanced breast cancer: SERENA-1 monotherapy results. Ann Oncol. 2024;35:707–17. https://doi.org/10.1016/j.annonc.2024.04.012.
8. Pathak N, Oliveira M. New oral selective Estrogen receptor degraders redefine management of Estrogen receptor-Positive breast cancer. Annu Rev Med. 2025;76:243–55. https://doi.org/10.1146/annurev-med-052423-122001.
9. Jhaveri KL, Neven P, Casalnuovo ML, Kim SB, Tokunaga E, Aftimos P, Saura C, O'Shaughnessy J, Harbeck N, Carey LA, Curigliano G, Llombart-Cussac A, Lim E, Garcia Tinoco ML, Sohn J, Mattar A, Zhang Q, Huang CS, Hung CC, Martinez Rodriguez JL, Ruiz Borrego M, Nakamura R, Pradhan KR, von Cramer C, Barrett E, Cao S, Wang XA, Smyth LM. Bidard FC and group E-S 2025 imlunestrant with or without abemaciclib in advanced breast cancer. N Engl J Med. 392:1189–202. https://doi.org/10.1056/NEJMoa2410858.
10. Keam SJ. Imlunestrant: First Approval. Drugs. 2025. https://doi.org/10.1007/s40265-025-02266-x. Epub ahead of print.
11. Cipolletti M, Bartoloni S, Busonero C, Parente M, Leone S, Acconcia F. A new anti-estrogen discovery platform identifies FDA-approved imidazole anti-fungal drugs as bioactive compounds against ERα expressing breast cancer cells. Int J Mol Sci. 2021. https://doi.org/10.3390/ijms22062915.
12. Bartoloni S, Leone S, Pescatori S, Cipolletti M, Acconcia F. The antiviral drug Telaprevir induces cell death by reducing FOXA1 expression in Estrogen receptor alpha (ERalpha)-positive breast cancer cells. Mol Oncol. 2022;16:3568–84. https://doi.org/10.1002/1878-0261.13303.
13. Busonero C, Leone S, Bianchi F, Maspero E, Fiocchetti M, Palumbo O, et al. Ouabain and digoxin activate the proteasome and the degradation of the ERα in cells modeling primary and metastatic breast cancer. Cancers (Basel). 2020. https://doi.org/10.3390/cancers12123840.
14. Pescatori S, Leone S, Cipolletti M, Bartoloni S, di Masi A, Acconcia F. Clinically relevant CHK1 inhibitors abrogate wild-type and Y537S mutant ERα expression and proliferation in luminal primary and metastatic breast cancer cells. J Exp Clin Cancer Res. 2022;41:27. https://doi.org/10.1186/s13046-022-02360-y.
15. Dustin D, Gu G, Fuqua SAW. *ESR1* mutations in breast cancer. Cancer. 2019;125:3714–28. https://doi.org/10.1002/cncr.32345.
16. Irani S, Tan W, Li Q, Toy W, Jones C, Gadiya M, et al. Somatic estrogen receptor α mutations that induce dimerization promote receptor activity and breast cancer proliferation. J Clin Invest. 2024. https://doi.org/10.1172/JCI163242.
17. Kingston B, Pearson A, Herrera-Abreu MT, Sim LX, Cutts RJ, Shah H, et al. *ESR1* F404 mutations and acquired resistance to fulvestrant in *ESR1*-mutant breast cancer. Cancer Discov. 2024;14:274–89. https://doi.org/10.1158/2159-8290.CD-22-1387.
18. Pavlin M, Spinello A, Pennati M, Zaffaroni N, Gobbi S, Bisi A, et al. A computational assay of Estrogen Receptor α antagonists reveals the key common structural traits of drugs effectively fighting refractory breast cancers. Sci Rep. 2018;8:649. https://doi.org/10.1038/s41598-017-17364-4.
19. Brzozowski AM, Pike AC, Dauter Z, Hubbard RE, Bonn T, Engstrom O, et al. Molecular basis of agonism and antagonism in the oestrogen receptor. Nature. 1997;389:753–8. https://doi.org/10.1038/39645.
20. Harrod A, Fulton J, Nguyen VTM, Periyasamy M, Ramos-Garcia L, Lai CF, et al. Genomic modelling of the ESR1 Y537S mutation for evaluating function and new therapeutic approaches for metastatic breast cancer. Oncogene. 2017;36:2286–96. https://doi.org/10.1038/onc.2016.382.
21. Bartoloni S, Pescatori S, Bianchi F, Cipolletti M, Acconcia F. Selective impact of ALK and MELK inhibition on ERα stability and cell proliferation in cell lines representing distinct molecular phenotypes of breast cancer. Sci Rep. 2024;14:8200. https://doi.org/10.1038/s41598-024-59001-x.
22. Srinivas H, Juroske DM, Kalyankrishna S, Cody DD, Price RE, Xu XC, et al. C-Jun N-terminal kinase contributes to aberrant retinoid signaling in lung cancer cells by phosphorylating and inducing proteasomal degradation of retinoic acid receptor alpha. Mol Cell Biol. 2005;25:1054–69. https://doi.org/10.1128/MCB.25.3.1054-1069.2005.
23. Totta P, Pesiri V, Enari M, Marino M, Acconcia F. Clathrin heavy chain interacts with Estrogen receptor alpha and modulates 17beta-estradiol signaling. Mol Endocrinol. 2015;29:739–55. https://doi.org/10.1210/me.2014-1385.
24. Cipolletti M, Leone S, Bartoloni S, Busonero C, Acconcia F. Real-time measurement of E2: ERalpha transcriptional activity in living cells. J Cell Physiol. 2020. https://doi.org/10.1002/jcp.29565.
25. Cipolletti M, Pescatori S, Acconcia F. Real-time challenging of ERα Y537S mutant transcriptional activity in living cells. Endocrines. 2021;2:54–64. https://doi.org/10.3390/endocrines2010006.
26. Toy W, Shen Y, Won H, Green B, Sakr RA, Will M, Li Z, Gala K, Fanning S, King TA, Hudis C, Chen D, Taran T, Hortobagyi G, Greene G, Berger M, Baselga J, Chandarlapaty S. ESR1 ligand-binding domain mutations in hormone-resistant breast cancer. Nat Genet. 2013;45:1439–45. https://doi.org/10.1038/ng.2822.
27. Hoffman LM, Garcha K, Karamboulas K, Cowan MF, Drysdale LM, Horton WA, et al. BMP action in skeletogenesis involves attenuation of retinoid signaling. J Cell Biol. 2006;174:101–13. https://doi.org/10.1083/jcb.200604150.
28. Rafii P, Seibel C, Weitz HT, Ettich J, Minafra AR, Petzsch P, et al. Cytokimera GIL-11 rescued IL-6R deficient mice from partial hepatectomy-induced death by signaling via non-natural gp130:LIFR:IL-11R complexes. Commun Biol. 2023;6:418. https://doi.org/10.1038/s42003-023-04768-4.
29. Nikolovska-Coleska Z, Wang R, Fang X, Pan H, Tomita Y, Li P, Roller PP, Krajewski K, Saito NG, Stuckey JA, Wang S. Development and optimization of a binding assay for the XIAP BIR3 domain using fluorescence polarization. Anal Biochem. 2004;332:261–73. https://doi.org/10.1016/j.ab.2004.05.055.
30. Cheng Y, Prusoff WH. Relationship between the inhibition constant (K1) and the concentration of inhibitor which causes 50 per cent inhibition (I50) of an enzymatic reaction. Biochem Pharmacol. 1973;22:3099–108. https://doi.org/10.1016/0006-2952(73)90196-2.
31. Case DAea. 2020 AMBER 2020. University of California, San Francisco. https://ambermd.org/.
32. Tian C, Kasavajhala K, Belfon KAA, Raguette L, Huang H, Migues AN, et al. Ff19SB: amino-acid-specific protein backbone parameters trained against quantum mechanics energy surfaces in solution. J Chem Theory Comput. 2020;16:528–52. https://doi.org/10.1021/acs.jctc.9b00591.
33. Darden TY, Pedersen L. Particle mesh Ewald: an N·log(N) method for Ewald sums in large systems. J Chem Phys. 1993. https://doi.org/10.1063/1.464397.
34. Grest GS, Kremer K. Molecular dynamics simulation for polymers in the presence of a heat bath. Phys Rev Gen Phys. 1986;33:3628–31. https://doi.org/10.1103/physreva.33.3628.
35. Berendsen HJCP, van Gunsteren WF, Di Nola A, Haak JR. Molecular dynamics with coupling to an external bath. J Chem Phys. 1984;81:3684–90. https://doi.org/10.1063/1.448118.
36. Rickaert J-PC, Berendsen G, H.J.C. Numerical integration of the cartesian equations of motion of a system with constraints: molecular dynamics of n-alkanes. J Comput Phys. 1977;23:327–41. https://doi.org/10.1016/0021-9991(77)90098-5.
37. Case DAea. 2022 AmberTools22. University of California, San Francisco. https://ambermd.org/.
38. La Rosa P, Pesiri V, Marino M, Acconcia F. 17 beta-Estradiol-induced cell proliferation requires Estrogen receptor (ER) alpha monoubiquitination. Cell Signal. 2011;23:1128–35. https://doi.org/10.1016/j.cellsig.2011.02.006.

39. Leone S, Busonero C, Acconcia F. A high throughput method to study the physiology of E2:ERalpha signaling in breast cancer cells. J Cell Physiol. 2018;233:3713–22. https://doi.org/10.1002/jcp.26251.
40. Katzenellenbogen JA, Mayne CG, Katzenellenbogen BS, Greene GL, Chandarlapaty S. Structural underpinnings of oestrogen receptor mutations in endocrine therapy resistance. Nat Rev Cancer. 2018;18:377–88. https://doi.org/10.1038/s41568-018-0001-z.
41. Cipolletti M, Acconcia F. <article-title update="added">PMM2 controls ERα levels and cell proliferation in ESR1 Y537S variant expressing breast cancer cells. Mol Cell Endocrinol. 2024;584:112160. https://doi.org/10.1016/j.mce.2024.112160.
42. Harrod A, Lai CF, Goldsbrough I, Simmons GM, Oppermans N, Santos DB, et al. Genome engineering for estrogen receptor mutations reveals differential responses to anti-estrogens and new prognostic gene signatures for breast cancer. Oncogene. 2022;41:4905–15. https://doi.org/10.1038/s41388-022-02483-8.
43. La Rosa P, Pesiri V, Leclercq G, Marino M, Acconcia F. Palmitoylation regulates 17beta-estradiol-induced estrogen receptor-alpha degradation and transcriptional activity. Mol Endocrinol. 2012;26:762–74. https://doi.org/10.1210/me.2011-1208.
44. Acconcia F, Fiocchetti M, Busonero C, Fernandez VS, Montalesi E, Cipolletti M, et al. The extra-nuclear interactome of the estrogen receptors: implications for physiological functions. Mol Cell Endocrinol. 2021;538:111452. https://doi.org/10.1016/j.mce.2021.111452.
45. Mortazavi A, Williams BA, McCue K, Schaeffer L, Wold B. Mapping and quantifying mammalian transcriptomes by RNA-Seq. Nat Methods. 2008;5:621–8. https://doi.org/10.1038/nmeth.1226.
46. Trapnell C, Williams BA, Pertea G, Mortazavi A, Kwan G, van Baren MJ, et al. Transcript assembly and quantification by RNA-Seq reveals unannotated transcripts and isoform switching during cell differentiation. Nat Biotechnol. 2010;28:511–5. https://doi.org/10.1038/nbt.1621.
47. Liberzon A, Birger C, Thorvaldsdottir H, Ghandi M, Mesirov JP, Tamayo P. The molecular signatures database (MSigDB) hallmark gene set collection. Cell Syst. 2015;1:417–25. https://doi.org/10.1016/j.cels.2015.12.004.
48. Li Z, Li T, Yates ME, Wu Y, Ferber A, Chen L, et al. The EstroGene database reveals diverse temporal, context-dependent, and bidirectional estrogen receptor regulomes in breast cancer. Cancer Res. 2023;83:2656–74. https://doi.org/10.1158/0008-5472.CAN-23-0539.
49. Shiau AK, Barstad D, Loria PM, Cheng L, Kushner PJ, Agard DA, et al. The structural basis of estrogen receptor/coactivator recognition and the antagonism of this interaction by tamoxifen. Cell. 1998;95:927–37. https://doi.org/10.1016/s0092-8674(00)81717-1.
50. Pavlin M, Gelsomino L, Barone I, Spinello A, Catalano S, Ando S, et al. <article-title update="added">Structural, thermodynamic, and kinetic traits of antiestrogen-compounds selectively targeting the Y537S mutant estrogen receptor α transcriptional activity in breast cancer cell lines. Front Chem. 2019;7:602. https://doi.org/10.3389/fchem.2019.00602.
51. Lavudi K, Nuguri SM, Olverson Z, Dhanabalan AK, Patnaik S, Kokkanti RR. Targeting the retinoic acid signaling pathway as a modern precision therapy against cancers. Front Cell Dev Biol. 2023;11:1254612. https://doi.org/10.3389/fcell.2023.1254612.
52. Shilkaitis A, Green A, Christov K. Retinoids induce cellular senescence in breast cancer cells by RAR-beta dependent and independent pathways: potential clinical implications (review). Int J Oncol. 2015;47:35–42. https://doi.org/10.3892/ijo.2015.3013.
53. Blackford AN, Jackson SP. ATM, ATR, and DNA-PK: the trinity at the heart of the DNA damage response. Mol Cell. 2017;66:801–17. https://doi.org/10.1016/j.molcel.2017.05.015.
54. Hernandez-Segura A, Nehme J, Demaria M. Hallmarks of cellular senescence. Trends Cell Biol. 2018;28:436–53. https://doi.org/10.1016/j.tcb.2018.02.001.
55. Milczarek M. The premature senescence in breast cancer treatment strategy. Cancers (Basel). 2020. https://doi.org/10.3390/cancers12071815.
56. Hua S, Kittler R, White KP. Genomic antagonism between retinoic acid and estrogen signaling in breast cancer. Cell. 2009;137:1259–71. https://doi.org/10.1016/j.cell.2009.04.043.
57. Ross-Innes CS, Stark R, Holmes KA, Schmidt D, Spyrou C, Russell R, et al. Cooperative interaction between retinoic acid receptor-alpha and estrogen receptor in breast cancer. Genes Dev. 2010;24:171–82. https://doi.org/10.1101/gad.552910.
58. Metivier R, Penot G, Hubner MR, Reid G, Brand H, Kos M, Gannon. F 2003 Estrogen receptor-alpha directs ordered, cyclical, and combinatorial recruitment of cofactors on a natural target promoter. Cell 115:751–63. https://doi.org/S0092867403009346.
59. Reid G, Hubner MR, Metivier R, Brand H, Denger S, Manu D, Beaudouin J, Ellenberg J, Gannon F. 2003 Cyclic, proteasome-mediated turnover of unliganded and liganded ERalpha on responsive promoters is an integral feature of estrogen signaling. Mol Cell 11:695–707. https://doi.org/S109727650300090X.
60. Wang L, Lankhorst L, Bernards R. Exploiting senescence for the treatment of cancer. Nat Rev Cancer. 2022;22:340–55. https://doi.org/10.1038/s41568-022-00450-9.
61. Guerrero A, Herranz N, Sun B, Wagner V, Gallage S, Guiho R, et al. Cardiac glycosides are broad-spectrum senolytics. Nat Metab. 2019;1:1074–88. https://doi.org/10.1038/s42255-019-0122-z.
62. La Rosa P, Marino M, Acconcia F. 17 beta-estradiol regulates estrogen receptor alpha monoubiquitination. IUBMB Life. 2011;63:49–53. https://doi.org/10.1002/iub.414.
63. Blair IA. Analysis of estrogens in serum and plasma from postmenopausal women: past present, and future. Steroids. 2010;75:297–306. https://doi.org/10.1016/j.steroids.2010.01.012.
64. Bense RDdV EGE, Schroder CP, Fermann RSN. Higher expression of Estrogen response genes in the primary tumor is associated with a greater risk for late recurrence in patients with ER+/HER2-breast cancer. Breast Cancer Early Stage. 2017;28. https://doi.org/10.1093/annonc/mdx362.046.
65. Lee N, Park MJ, Song W, Jeon K, Jeong S. Currently applied molecular assays for identifying ESR1 mutations in patients with advanced breast cancer. Int J Mol Sci. 2020. https://doi.org/10.3390/ijms21228807.
66. Lukasiewicz S, Czeczelewski M, Forma A, Baj J, Sitarz R, Stanislawek. A 2021 breast Cancer-Epidemiology, risk Factors, Classification, prognostic Markers, and current treatment Strategies-An updated review. Cancers (Basel) 13. https://doi.org/10.3390/cancers13174287.
67. Wander SA, Cohen O, Gong X, Johnson GN, Buendia-Buendia JE, Lloyd MR, et al. The genomic landscape of intrinsic and acquired resistance to cyclin-dependent kinase 4/6 inhibitors in patients with hormone receptor-positive metastatic breast cancer. Cancer Discov. 2020;10:1174–93. https://doi.org/10.1158/2159-8290.CD-19-1390.
68. Lefebvre C, Bachelot T, Filleron T, Pedrero M, Campone M, Soria JC, et al. Mutational profile of metastatic breast cancers: a retrospective analysis. PLoS Med. 2016;13:e1002201. https://doi.org/10.1371/journal.pmed.1002201.
69. Garcia-Recio S, Hinoue T, Wheeler GL, Kelly BJ, Garrido-Castro AC, Pascual T, et al. Multiomics in primary and metastatic breast tumors from the AURORA US network finds microenvironment and epigenetic drivers of metastasis. Nat Cancer. 2023;4:128–47. https://doi.org/10.1038/s43018-022-00491-x.
70. Pleasance E, Titmuss E, Williamson L, Kwan H, Culibrk L, Zhao EY, et al. Pan-cancer analysis of advanced patient tumors reveals interactions between therapy and genomic landscapes. Nat Cancer. 2020;1:452–68. https://doi.org/10.1038/s43018-020-0050-6.
71. Wang P, Bahreini A, Gyanchandani R, Lucas PC, Hartmaier RJ, Watters RJ, et al. Sensitive detection of mono- and polyclonal ESR1 mutations in primary tumors, metastatic lesions, and cell-free DNA of breast cancer patients. Clin Cancer Res. 2016;22:1130–7. https://doi.org/10.1158/1078-0432.CCR-15-1534.
72. Li Z, Chen F, Chen L, Liu J, Tseng D, Hadi F, et al. The EstroGene2.0 database for endocrine therapy response and resistance in breast cancer. NPJ Breast Cancer. 2024;10:106. https://doi.org/10.1038/s41523-024-00709-4.
73. Stork CT, Bocek M, Crossley MP, Sollier J, Sanz LA, Chedin F, et al. Co-transcriptional R-loops are the main cause of estrogen-induced DNA damage. Elife. 2016. https://doi.org/10.7554/eLife.17548.
74. Pescatori S, Berardinelli F, Albanesi J, Ascenzi P, Marino M, Antoccia A, et al. A Tale of Ice and Fire: The Dual Role for 17β-Estradiol in Balancing DNA Damage and Genome Integrity. Cancers (Basel). 2021. https://doi.org/10.3390/cancers13071583.
75. Nagai Y, Ambinder AJ. The Promise of Retinoids in the Treatment of Cancer: Neither Burnt Out Nor Fading Away. Cancers (Basel). 2023. https://doi.org/10.3390/cancers15143535.
76. Costantini L, Molinari R, Farinon B, Merendino N. Retinoic Acids in the Treatment of Most Lethal Solid Cancers. J Clin Med. 2020. https://doi.org/10.3390/jcm9020360.

77. Garattini E, Bolis M, Garattini SK, Fratelli M, Centritto F, Paroni G, et al. Retinoids and breast cancer: from basic studies to the clinic and back again. Cancer Treat Rev. 2014;40:739. https://doi.org/10.1016/j.ctrv.2014.01.001.